

ForestScan: a unique multiscale dataset of tropical forest structure across 3 continents including terrestrial, UAV and airborne LiDAR and in-situ forest census data

Cecilia Chavana-Bryant^{1,2}, Phil Wilkes^{1,2,24}, Wanxin Yang^{1,2}, Andrew Burt³, Peter Vines¹⁹, Amy C. Bennett⁴, Georgia C. Pickavance⁴, Declan L. M. Cooper^{1,25}, Simon L. Lewis^{1,4}, Oliver L. Phillips⁴, Benjamin Brede⁵, Alvaro Lau¹¹, Martin Herold⁵, Iain M. McNicol⁶, Edward T.A. Mitchard^{6,18}, David A. Coomes⁸, Toby D. Jackson⁸, Löic Makaga⁹, Heddy O. Milamizokou Napo⁹, Alfred Ngomanda¹⁵, Stephan Ntie⁹, Vincent Medjibe⁹, Pacôme Dimbonda⁹, Luna Soenens¹⁰, Virginie Daelemans²³, Laetitia Proux¹³, Reuben Nilus¹², Nicolas Labrière²⁰, Kathryn Jeffery^{14, 17}, David F.R.P. Burslem²¹, Dan Clewley¹⁶, David Moffat¹⁶, Lan Qie²², Harm Bartholomeus¹¹, Gregoire Vincent⁷, Nicolas Barbier⁷, Geraldine Derroire¹³, Katharine Abernethy^{14,15}, Klaus Scipal¹⁷ and Mathias Disney^{1,2}

¹Department of Geography, University College London, London, WC1E 6BT, UK

²NERC National Centre for Earth Observation, UCL Geography, London, WC1E 6BT, UK

³Sylvera Ltd., London, EC1Y 4TW, UK

⁴School of Geography, University of Leeds, Leeds, LS2 9JT, UK

⁵Section 1.4 Remote Sensing and Geoinformatics, GFZ Helmholtz Centre for Geosciences, Potsdam, 14473, DE

⁶School of GeoSciences, University of Edinburgh, Edinburgh, EH9 3JN, UK

⁷AMAP, Univ. Montpellier, CIRAD, CNRS, INRAE, IRD, Montpellier, 34398, FR

⁸Plant Science and Cambridge Conservation Initiative, University of Cambridge, Cambridge, CB2 3QZ, UK

⁹Agence Nationale des Parcs Nationaux (ANPN), PO Box 20379, Libreville, GA

¹⁰Q-ForestLab, Department of Environment, Ghent University, Coupure Links 653, B-9000, Ghent, BE
11¹¹U.S. Environmental Protection Agency, Washington, DC 20460, USA

¹¹Laboratory of Geo-Information Science and Remote Sensing, Wageningen University & Research, 6708 PB Wageningen, NL

¹²Forest Research Centre, Sabah Forestry Department, P.O. Box 1407, Sabah, 90715, MY

¹⁵CIRAD, UMR EcoFoG (AgroParistech, CNRS, INRAE, Université des Antilles, Université de Guyane), Campus Agronomique, Kourou, 20040, FG

¹⁴Faculty of Natural Sciences, University of Stirling, Stirling, FK9 4LA, UK

¹⁵Institut de Recherche en Ecologie Tropicale, IRET/CENAREST, Libreville, PO Box 13354, GA
(P.O. Box 13354, Libreville, Gabon)

¹⁷ESRI, *MapServer*, ESRI, Redlands, CA, USA.

¹⁷ESA Centre for Earth Observation (ESA-ESRIN), Frascati, 00044, IT
¹⁸Green, J. J., Lillie, J. J., 1993, Green Street, Edgbaston, B15 2ES, UK

¹⁸Space Intelligence Ltd. 93 George Street, Edinburgh, EH2 3ES, UK
¹⁹22, 1, 1, T, Bl, 41, BL2 1AT, UK

¹⁸ Havelock Terrace, Plymouth, PL2 1AT, UK

²⁰Centre de Recherche sur la Biodiversité et l'Environnement (CRBE), UMR 5300 CNRS-IRD-INP-U13, Toulouse, 31062 cedex 9, FR

²¹School of Biological Sciences, University of Aberdeen, Aberdeen, AB24 3UU, UK

²²College of Health and Science, Department of Life Sciences, University of Lincoln, Lincoln, LN6 7TS, UK

²²Gembloux Agro-Bio Tech Liege University, Passage des deportes 2, B-5030 Gembloux, BE
²³Walsham, Andover, West Sussex, BH12 7TQ, UK

²⁵Centre for Biodiversity and Environment Research, Department of Biological Sciences, University of East Anglia, Norwich, UK.

Centre for Biodiversity and Environment Research, Department of Environment, London, WC1E 6BT, UK

London, London, WC1E 6BT, UK

Correspondence to: Dr Cecilia Cha

41 **Abstract**

42 The ForestScan project was conceived to evaluate new technologies for characterising forest structure and biomass at Forest
43 Biomass Reference Measurement Sites (FBRMS). It is closely aligned with other international initiatives, particularly the
44 Committee on Earth Observation Satellites (CEOS) Working Group on Calibration & Validation (WGCV) aboveground
45 biomass (AGB) cal/val protocols, and is part of GEO-TREES, an international consortium dedicated to establishing a global
46 network of Forest Biomass Reference Measurement Sites (FBRMS) to support EO and encourage investment in relevant field-
47 based observations and science. ForestScan is the first demonstration of what can be achieved more broadly under GEO-
48 TREES, which would significantly expand and enhance the use of EO-derived AGB estimates.

49

50 We present data from the ForestScan project, a unique multiscale dataset of tropical forest three-dimensional (3D) structural
51 measurements, including terrestrial laser scanning (TLS), unpiloted aerial vehicle laser scanning (UAV-LS), airborne laser
52 scanning (ALS), and in-situ tree census and ancillary data. These data are critical for the calibration and validation of EO
53 estimates of forest biomass, as well as providing broader insights into tropical forest structure.

54

55 Data are presented for three FBRMS: FBRMS-01: Paracou, French Guiana; FBRMS-02: Lopé, Gabon; and FBRMS-03:
56 Kabilis-Sepilok, Malaysia. Field data for each site include new 3D LiDAR measurements combined with plot tree census and
57 ancillary data, at a multi-hectare scale. Not all data types were collected at all sites, reflecting the practical challenges of field
58 data collection. We also provide detailed data collection protocols and recommendations for TLS, UAV-LS, ALS and plot
59 census measurements for each site, along with requirements for ancillary data to enable integration with ALS data (where
60 possible) and upscaling to EO estimates. We outline the requirements and challenges for field data collection for each data
61 type and discuss the practical considerations for establishing new FBRMS or upgrading existing sites to FBRMS standard,
62 including insights into the associated costs and benefits.

63 **1. Introduction**

64 Our capability to estimate forest structure and AGB has rapidly advanced, leveraging new remote sensing observations from
65 ground, air, and space. This progress underscores the importance of quantifying and understanding terrestrial carbon sources
66 and sinks, the response of global forests to climate change, and conservation and restoration efforts at local to global scales.
67 These new measurements broadly fall into the following categories:

68

69 1) TLS provides highly detailed (centimetre-scale) 3D structural measurements across hectare scales, enabling non-
70 destructive AGB estimates that are independent of, yet complementary to, empirical allometric model estimates (e.g.
71 Calders et al., 2022; Demol et al., 2024).

72

73 2) UAV-LS has evolved from highly specialised and expensive surveying platforms to more operational, low-cost
74 systems that offer coverage of several to thousands of hectares, with hundreds to thousands of points per square metre
75 from above. These data can be used to estimate forest canopy height, basal area, tree crown size and shape, vertical
76 structure, and AGB via allometric model functions of tree properties, including height, diameter at breast height
77 (DBH), and crown shape (Brede et al., 2022a; Kellner et al., 2019) However, as UAV-LS systems proliferate, the
78 need for intercalibration between sensors increases, due to differences in scanner and laser properties such as power,
79 wavelength, divergence, and scan rate, which result in notable variations in penetration and object detection rates
80 (Vincent et al., 2023).

81
82 3) Airborne laser scanning (ALS) has been a well-established tool in forestry and forest ecology since the 1990s. ALS
83 is routinely used to estimate forest height, structure, and AGB at stand level via empirical models and at regional to
84 national scales via allometric models (Duncanson et al., 2019; Jucker et al., 2017).

85
86 4) Spaceborne Light Detection and Ranging (Spaceborne LiDAR) (e.g. GEDI, ICESat, and ICESat-2) can provide
87 estimates of forest height in non-continuous footprints of tens to hundreds of metres, underpinning most large-scale
88 AGB maps, particularly in the lowland tropics (Avitabile et al., 2011; Avitabile et al., 2016; Saatchi et al., 2011).
89 Various satellite missions have also provided empirical evidence for correlations between the radar signal and AGB
90 for AGB < 250 Mg ha⁻¹ (Askne and Santoro, 2012), but the ESA BIOMASS mission, launched on the 29th of April
91 2025, is the only mission specifically targeting higher biomass tropical forests (Quegan et al., 2019; Ramachandran
92 et al., 2023).

93
94 The current challenge is to consistently collect and process plot-based measurements in support of EO-derived AGB, combine
95 them, integrate them with long-term ground-based inventory approaches, and optimally use them with EO data. There is
96 increasing recognition that the value of large-scale EO approaches to assessing AGB and forest structure largely depends on
97 robust calibration and validation data (Duncanson et al., 2019; Nature Editorial, 2022; Ochiai et al., 2023). This knowledge
98 and capability gap have led to calls for concerted international funding and coordination to establish long-term Forest Biomass
99 Reference Measurement Sites (FBRMS), with a particular focus on tropical forests (Labrière et al., 2023; Schepaschenko et
100 al., 2019).

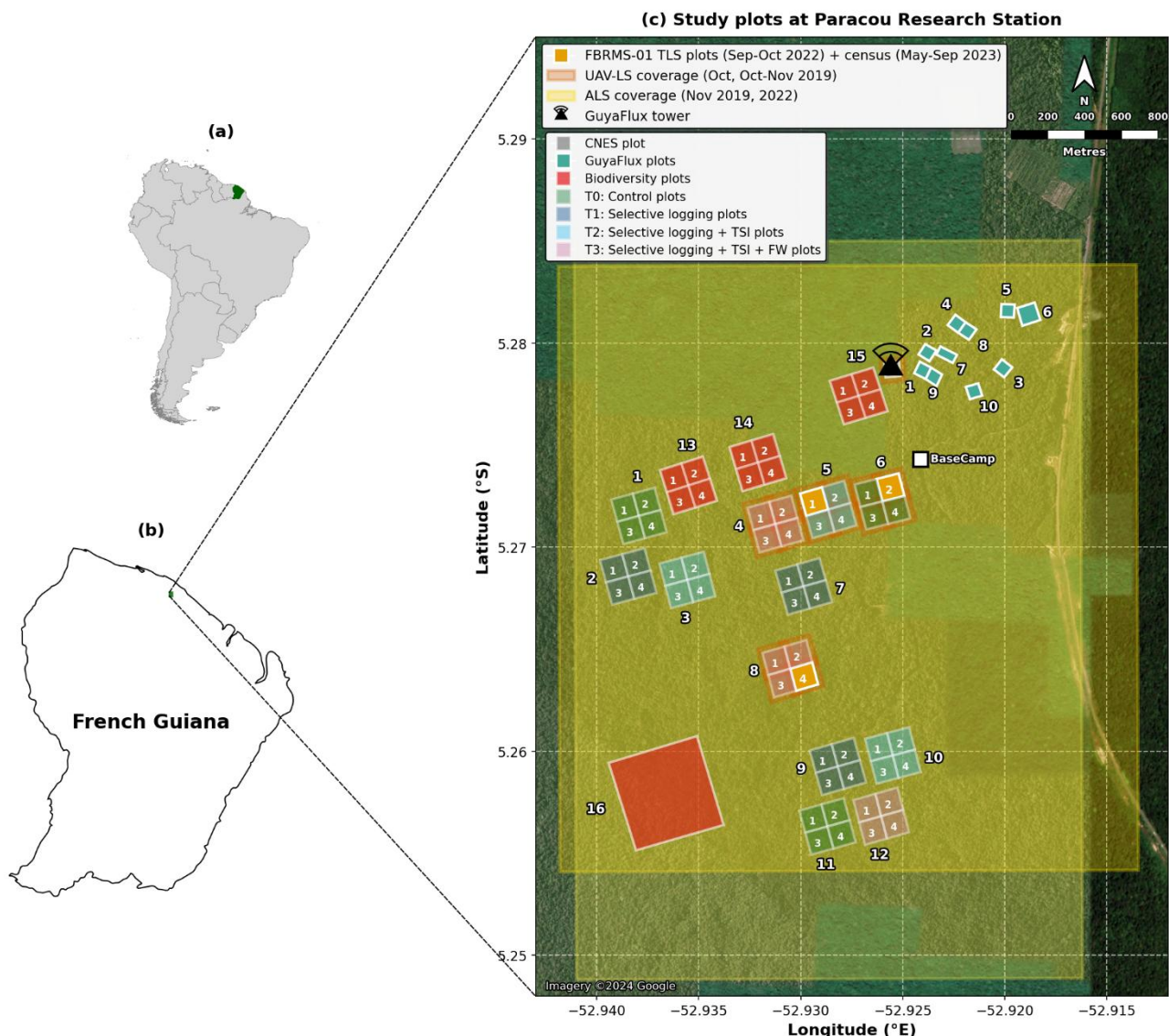
101
102 Here, we present a new dataset from the European Space Agency (ESA) funded ForestScan project, which contributes to this
103 aim and provides access to data from the first three FBRMS of the GEO-TREES network. The project has collected data,
104 including TLS, UAV-LS, ALS, and census data, covering three FBRMS across the tropics. We describe these data, related
105 data collection and processing protocols and tools, and make brief recommendations for future data collection for FBRMS.

106 **2. Methodology**

107 **2.1 ForestScan Forest Biomass Reference Measurement Sites (FBRMS)**

108 Three Forest Biomass Research Monitoring Sites (FBRMS) were selected based on various criteria, including the availability
109 of well-established plots, the representativity of tropical forest types and climates, established collaborations, agreements and
110 logistical support with in-country partners, and the availability of previously collected data, particularly census data, as well
111 as ALS and TLS data. The chosen sites were:

112 • FBRMS-01: Paracou Research Station, French Guiana
113 • FBRMS-02: Station d'Etudes des Gorilles et Chimpanzés, Lopé National Park, Gabon
114 • FBRMS-03: Kabili-Sepilok, Malaysian Borneo



117 **Figure 1:** Multi-scale map depicting the location and spatial distribution of research plots at Paracou Research Station, French
 118 Guiana. (a) Location of French Guiana (green) within South America. (b) Location of Paracou Research Station (green) within
 119 French Guiana. (c) Detailed site map showing the spatial distribution of research plots with treatment-specific colours, UAV-
 120 LS coverage (orange), and ALS coverage (yellow). The map displays 15 experimental 4 ha plots, each containing four 1 ha
 121 subplots numbered 1 - 4 (60 subplots in total; plots 1 - 12: silvicultural treatments; plots 13 - 15: Biodiversity monitoring), one
 122 large 40 ha Biodiversity plot (plot 16; red), and 10 GuyaFlux plots (solid green). Treatment categories include: Biodiversity
 123 monitoring plots (plots 13, 14, 15, 16; red), T0 Control (plots 1, 6, 11; green), T1 Selective logging (plots 2, 7, 9; dark blue),

124 T2 Selective logging + thinning by timber stand improvement (TSI; plots 3, 5, 10; cyan), and T3 Selective logging + TSI +
125 fuelwood harvesting/FW (plots 4, 8, 12; pink). The three FBRMS-01 subplots -FG5c1 (subplot 1 of plot 5), FG6c2 (subplot 2
126 of plot 6), and FG8c4 (subplot 4 of plot 8)- are shown in solid orange and were surveyed using terrestrial laser scanning (TLS)
127 with corresponding tree census data. The GuyaFlux tower location is indicated by a black triangle with radiating transmission
128 waves, and the Base Camp location is marked with a white square. Scale bar: 800 m. Map data: Natural Earth 10 m cultural
129 vectors. Satellite imagery basemap: Imagery ©2024 Google. Map projection: WGS84 (EPSG:4326).

130

131

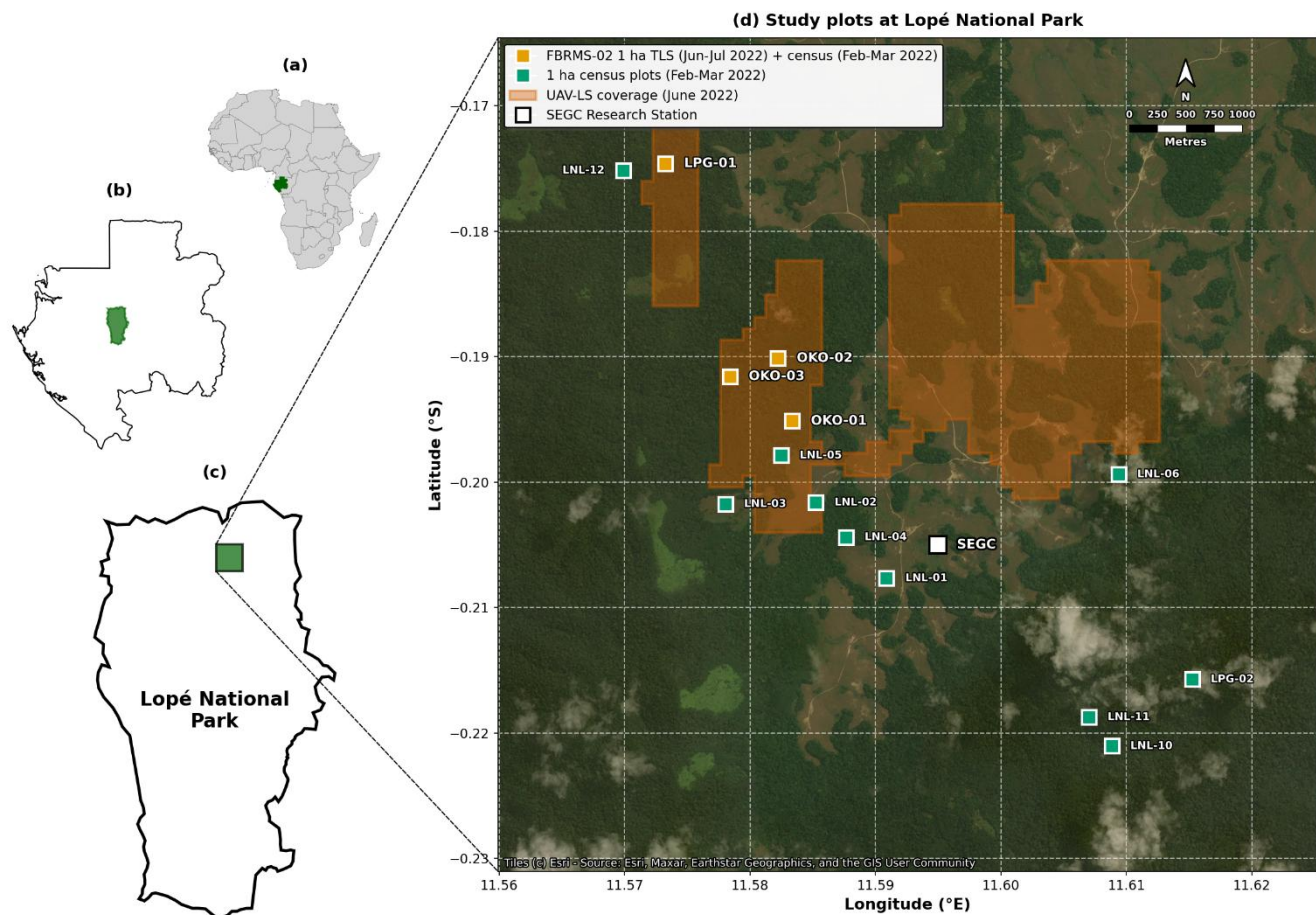
132 The Paracou research station is located near Sinnamary in the northern part of French Guiana, at a latitude of 5°18'N and a
133 longitude of 52°53'W. It is established on a long-term concession of the French National Centre for Space Studies (CNES)
134 and is managed by Centre de Coopération Internationale en Recherche Agronomique pour le Développement-Unité Mixte de
135 Recherche Écologie des Forêts de Guyane (Cirad-UMR EcoFoG). The station experiences an equatorial climate characterised
136 by two main climatic periods: a well-marked dry season from mid-August to mid-November and a long rainy season, often
137 interrupted by a short drier period between March and April. The station receives approximately 3,000 mm of rainfall annually
138 (mean annual precipitation from 2004 to 2014: 3,102 mm) and has a mean annual temperature of 25.7°C.

139

140 The core area of the Paracou research station (approximately 500 ha) is predominantly covered by lowland terra firme
141 rainforest. This old-growth forest has experienced no major human disturbance, although there are signs of pre-Columbian
142 activities. Species richness is high, with more than 750 woody species recorded, and 150 - 200 tree species per hectare with
143 DBH above 10 cm. A few dominant botanical families characterise the vegetation: Fabaceae, Chrysobalanaceae,
144 Lecythidaceae, Sapotaceae, and Burseraceae. The local heterogeneity of the floristic composition is mainly driven by soil
145 drainage. AGB, measured on trees with a DBH \geq 10 cm, ranges from 286.10 to 450 Mg/ha.

146

147 Following an initial inventory in the early 1980s, 12 permanent 6.25 ha plots were established in 1984. Plot corners, perimeters,
148 and inner trails (defining four subplots) were verified \sim 10 years later by a professional land surveyor. Nine plots were logged,
149 and six received additional silvicultural treatments between 1986 and 1988, creating a disturbance gradient with AGB losses
150 of 18–25% (treatment 1), 40–52% (treatment 2), and 48–58% (treatment 3). In the early 1990s, three more 6.25 ha plots and
151 one 25 ha plot were added, totalling \sim 120 ha of forest censused annually (controls), biennially (disturbed plots), or every five
152 years (25 ha plot). All 6.25 ha plots are subdivided into four subplots (see Fig. 1), with relative tree coordinates recorded. Trees
153 and palms \geq 10 cm DBH are mapped, identified, tagged, and periodically measured, forming a database of $>70,000$ trees. Since
154 2003, a 57 m flux tower has measured greenhouse gas fluxes, and an N, P, NP fertilisation experiment has been ongoing since
155 2015.



158 **Figure 2:** Multi-scale map showing the location and spatial distribution of research plots within Lopé National Park,
 159 Gabon. (a) Location of Gabon (green) within Africa. (b) Location of Lopé National Park (green) within Gabon. (c) Park
 160 boundary showing the research site location (green). (d) Detailed site map showing the spatial distribution of 14 one-hectare
 161 research plots. The four ForestScan FBRMS-02 plots (LPG-01, OKO-01, OKO-02, OKO-03; orange squares) were scanned
 162 using TLS during Jun-Jul 2022 with tree census data collected during Feb-Mar 2022. Tree census data was also collected for
 163 another ten plots (green circles) which are not part of the ForestScan project. Orange shaded areas indicate coverage of
 164 UAV-LS conducted in Jun 2022. The SEGC (Station d'Études des Gorilles et Chimpanzés) research station is marked with a
 165 yellow square. Map data: Natural Earth 10m cultural vectors. Satellite imagery basemap: Esri World Imagery (Esri, Maxar,
 166 Earthstar Geographics, and the GIS User Community). Map projection: WGS84 (EPSG:4326).

168 Lopé National Park is a 5000 km² protected area in central Gabon (Latitude 0°30'S
 169 and Longitude 11°30'E), comprising predominantly intact old-growth moist tropical forest. The northern part of the park
 170 features a savanna-forest mosaic, an anthropogenically maintained remnant of the landscape from the Last Glacial Maximum.
 171 The broader landscape is designated as a UNESCO World Heritage Site.

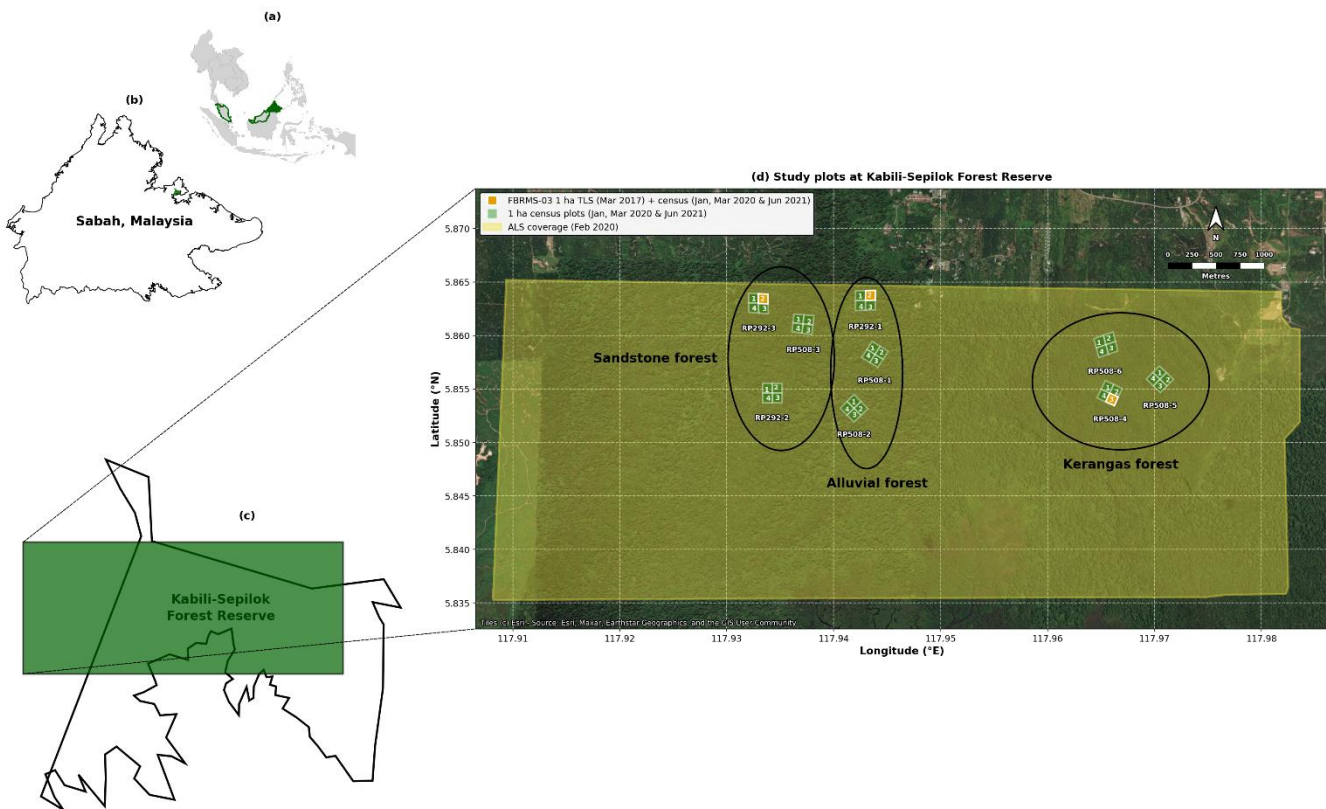
172

173 The transition from savanna to old-growth forest in the northern part of the park is characterised by six distinct forest types
 174 (Cuni-Sanchez et al., 2016; White et al., 1995): (i) savanna, (ii) colonising forest, (iii) monodominant Okoume forest, (iv)
 175 young Marantaceae forest, (v) mixed Marantaceae forest, and (vi) old-growth forest.

176

177 A substantial and varied body of literature has emerged from research conducted in Lopé National Park (Agence Nationale
 178 Des Parcs Nationaux, 2025). More than 100 long-term censused forest plots have been established within the park, contributing
 179 significant ground data for the calibration and validation of EO instruments (i.e. Duncanson et al., 2022; Saatchi et al., 2019).
 180 These plots also support various other research activities, such as the Global Ecosystem Monitoring (GEM) Network, an
 181 initiative aimed at understanding forest ecosystem functions and traits (Malhi et al., 2021).

182 **FBRMS-03: Kabil-Sepilok, Malaysian Borneo**



183

184 **Figure 3:** Multi-scale map showing the location and spatial distribution of research plots at Kabil-Sepilok Forest Reserve,
 185 Sabah, Malaysian Borneo. (a) Location of Sabah (green) within Malaysia (green boundary) in Southeast Asia.
 186 (b) Location of the Kabil-Sepilok Forest Reserve (green) within Sabah. (c) Kabil-Sepilok Forest Reserve area and site map area of panel
 187 d (green rectangle). (d) Detailed site map showing the spatial distribution of 9 x 4 ha plots (labelled RP291-1, RP292-3, etc.)

each containing four 1 ha subplots numbered 1 - 4 (36 subplots in total; green polygons with white subplot numbers) across three soil types: Alluvial forest, Sandstone forest, and Kerangas forest (delineated by black ellipses). The three FBRMS subplots are SEP-11 (subplot 2 of plot RP292-3, sandstone soil), SEP-12 (subplot 2 of plot RP292-1, alluvial soil) and SEP-30 (subplot 3 of plot RP508-4, kerangas soil). Three ForestScan FBRMS-03 1 ha subplots (orange polygons) were scanned using TLS during March 2017 and tree census for all subplots was collected in Jan, Mar of 2020 and Jun 2021. Yellow shading indicates ALS coverage acquired in February 2020. Scale bar: 1000 m. Map data: Natural Earth 10m cultural vectors. Satellite imagery basemap: Tiles ©Esri - Source: Esri, Maxar, Earthstar Geographics, and the GIS User Community. Map projection: WGS84 (EPSG:4326).

The Kabili-Sepilok Forest Reserve is located on the Sandakan Peninsula in North-East Sabah, Malaysia, and encompasses approximately 4,300 hectares of intact old-growth tropical forest. Sepilok has been protected since its establishment by the Sabah Forest Department in 1931. The elevation ranges from 50 to 250 metres above sea level. This topographic variation, combined with edaphic differences, results in three distinct forest types: (i) lowland mixed dipterocarp forest overlaying alluvial soil in the valleys, (ii) sandstone hill forest on hillsides and crests, and (iii) lowland mixed dipterocarp and kerangas forest at higher elevations (Sabah Forestry Department, n.d.).

Between 1995 and 2000, the Ecology Section of the Sabah Forestry Department established 36 one-hectare censused forest stands across these forest types, as illustrated in Fig. 3.

2.2 Data

2.2.1 Tree census

Quality-controlled, tree-by-tree data on identity (tag number and species) and diameter size for all sampled plots in each of the three FBRMS were collected using global standard tropical forest plot inventory protocols (Forestplots.Net et al., 2021). This ensured a consistent, full species-level census for all plot trees with a diameter equal to or greater than 10 cm at each FBRMS. Censuses provide tree-by-tree records that can potentially be linked to laser-scanning approaches. Species identity plays a key role in determining tree biomass through its strong influence on wood density. While laser-scanning techniques provide excellent measurements of tree dimensions (such as height and volume), they still require wood density estimates to convert these volumes into accurate biomass values (see Goodman et al., 2014). Census data also provide tree-by-tree measurements of tree diameter and whole forest basal area. Finally, because they are independent of constantly changing sensor technologies, when sustained over time, the core measurement protocols in forest plots deliver long-term consistency for tracking forest biomass change, growth, mortality, demography, and their trends over decades.

Census data for FBRMS plots in Gabon and Malaysia are available via ForestPlots.net (<https://forestplots.net/>, Forestplots.Net et al., 2021; Lopez-Gonzalez et al., 2011). ForestPlots.net is an internet-based facility with functionality to support all aspects of forest plot data management, including archiving, quality control, sharing, analysis, and data publishing via stable URLs (DOIs). ForestPlots.net currently supports the data management needs of more than 2,000 contributors working with 7,000

222 plots across 23 participating tropical networks. Data access requires potential users to provide details of their planned use and
223 agreement to abide by requirements for the inclusion of all contributing researchers. This encourages maximum inclusivity of
224 data originators and is recognised as a key part of what is required to maintain long-term investment in people and infrastructure
225 that enables continued measurements in these areas (De Lima et al., 2022).

226 **Tree census: FBRMS-01: Paracou, French Guiana**

227 In the Paracou FBRMS, tree censuses are conducted by two teams of three to five permanent field staff using Qfield on field
228 tablets (since 2020, field computers were used prior to this). Tree girth is measured with a measuring tape at 1.3 m, except
229 when buttresses necessitate a higher measurement point. The point of measurement (POM) is marked with paint to ensure the
230 exact same point of measurement between censuses. POM and its potential changes are recorded. New recruits -trees that have
231 grown beyond 10 cm DBH since the previous survey- are recorded by the field team using vernacular names, and their positions
232 are measured relative to the original trees. To ensure accurate identification, periodic botanical campaigns are conducted by
233 one or two experienced botanists, who also correct any misidentifications. When species cannot be identified in the field,
234 samples are collected and examined at the EcoFoG herbarium in Kourou or the IRD herbarium in Cayenne. All identifications
235 follow the Angiosperm Phylogeny Group (APG) IV plant classification system. Dead trees and the cause of their death are
236 recorded. Data are checked for errors after field census using an R script. Any abnormal measurement (e.g., girth showing
237 abnormal increase/decrease, missing value) is then rechecked in the field in the weeks following the initial census.

238
239 Plot descriptions for the Paracou FBRMS plots FG5c1, FG6c2 and FG8c4 are accessible via the Guyafor DataVerse
240 (<https://dataVERSE.cirad.fr>). This internet-based data repository provides plot descriptions and datasets downloadable as CSV
241 files, together with the corresponding metadata (Derroire et al., 2023). The ForestScan Project data package, including the
242 latest tree census data used in our analysis and collected in August 2023 for FBRMS plot FG5c1, in June 2023 for plot FG6c2,
243 and in September 2023 for plot FG8c4, is accessible via
244 <https://dataVERSE.cirad.fr/dataset.xhtml?persistentId=doi:10.18167/DVN1/94XHID> (Derroire et al., 2025).

245 **Tree census: FBRMS-02: Lopé, Gabon**

246 In the Lopé FBRMS, tree census data was collected at 12 plots in 2017 for the ESA AfriSAR campaign. During June - July
247 2022, these 13 plots plus one additional 1 ha plot (LPG-02) were re-censused, making a total of 11 x 1 ha forest plots, plus 3
248 x 1 ha plots in savanna (see Fig. 2). The 10 ha plots included LPG-01, OKO-01, OKO-02 and OKO-03, the 4 x 1 ha FBRMS
249 plots where TLS was conducted in 2017 and 2022.

250 **Tree census: FBRMS-03: Kibili-Sepilok, Malaysian Borneo**

251 In the Kibili-Sepilok FBRMS, tree census data was collected during 2020 - 2022 for a total of 9 x 4 ha plots (IDs RP291-1,
252 RP292-3, etc. see Fig. 3) each containing four 1 ha subplots numbered 1 – 4 and covering most of the long-term plots at this

253 site. The three FBRMS subplots SEP-11 (subplot 2 of plot RP292-3, sandstone soil), SEP-12 (subplot 2 of plot RP292-1, 254 alluvial soil) and SEP-30 (subplot 3 of plot RP508-4, kerangas soil) were scanned using TLS during March 2017 and tree 255 census for all subplots was collected in Jan, Mar of 2020 and Jun 2021. The 2020-2022 census was overdue as these plots had 256 not been censused since 2013.

257
258 Plot meta-data, including geography, institution, personnel and historical context, as well as tree-level census attributes (tag, 259 identity, diameter, point of measurement, stem condition, height, sub-plot, and, where measured x, y coordinates of 5 x 5 m 260 subplots) and multi-census attributes (tree demography and measurement trajectory and protocols, including growth, point of 261 measurement changes, recruitment, mortality, and mortality mode) were recorded for all Gabonese and Malaysian FBRMS 262 plots.

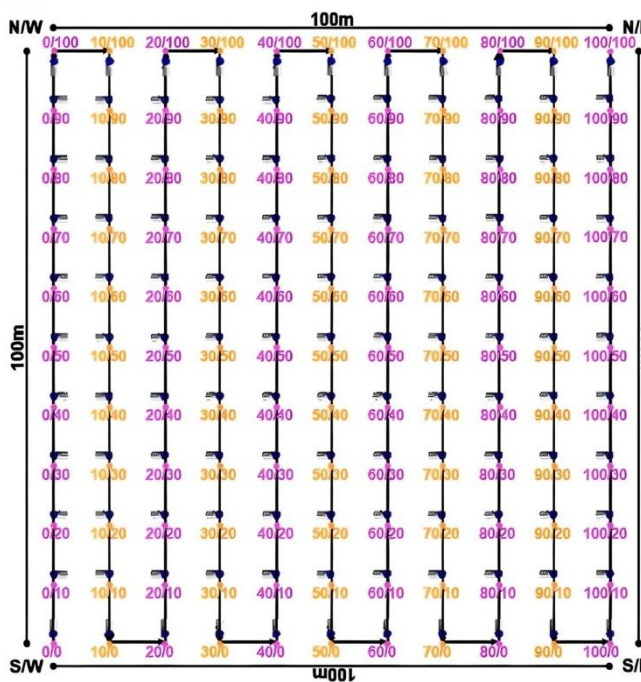
263
264 The ForestScan Project data package, includes data from the 2022 tree census collected during February and March for the 265 Gabon FBRMS plots and the Malaysian FBRMS plots census data collected in October 2020 for FBRMS plot SEP-11, in 266 March 2020 for plot SEP-12, and in June 2021 for plot SEP-30. This data package can be accessed via 267 https://doi.org/10.5521/forestplots.net/2025_2 (Chavana-Bryant et al., 2025).

268 **2.2.2 Terrestrial Laser Scanning (TLS)**

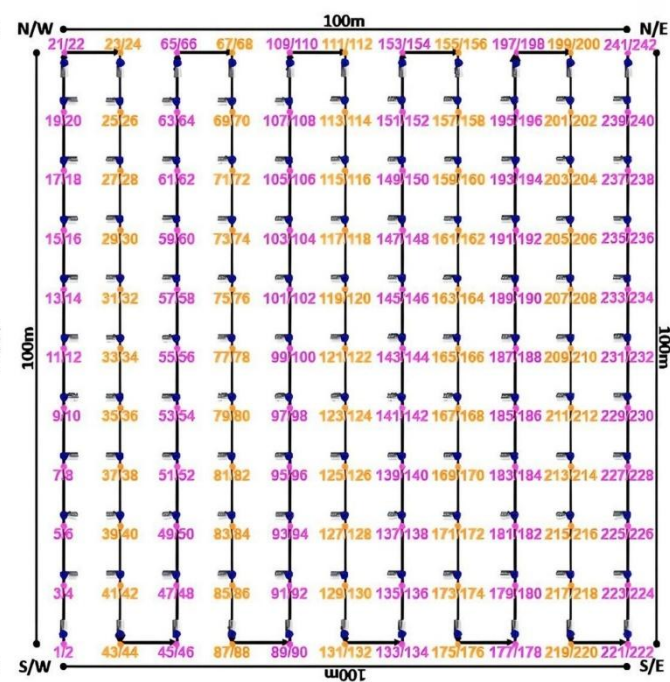
269 TLS data was collected to provide state-of-the-art estimates of tree- and stand-scale AGB for each FBRMS. These LiDAR 270 measurements, collected using the protocol described in the following sections, produce 3D point clouds with millimetre-level 271 accuracy representing the forest at each FBRMS. TLS chain sampling protocols (Wilkes et al., 2017), as illustrated and 272 described in Fig. 4, were employed at all three FBRMS. This data was processed to construct explicit Quantitative Structural 273 Models (QSMs) describing individual trees within each FBRMS with a DBH ≥ 10 cm. Tree- and stand-scale AGB estimates 274 were then calculated from the volumes of these models, using wood density values derived from published sources based on 275 species identification from botanical surveys.

276
277
278
279
280
281
282
283
284
285

(a)



(b)



289 **Figure 4:** TLS chain sampling was employed to capture high-quality LiDAR data suitable for accurate tree- and stand-scale
 290 AGB estimation. Chain sampling was deployed over a 10 m Cartesian grid, resulting in 11 sampling lines with 11 scan
 291 positions along each line (i.e., 0 – 10) within 1 ha forest plots. Sampling lines were established in a south-to-north direction
 292 (standard practice) and colour-coded using flagging tape, with the ID of each scan position written in permanent marker. Scan
 293 positions were identified by their line number and grid position, as shown in panel b (left). Due to the scanner's 100° field of
 294 view, capturing a complete scene at each scan position required two scans—upright and tilted. Consequently, 242 scans were
 295 collected from 121 positions at each 1 ha forest plot. The order in which the 242 individual scans were collected at each plot
 296 is depicted in panel b (right). The first scan at each plot was collected at the southwest corner, i.e., scan position 0,0 (unless
 297 impeded by obstacles such as streams, large tree falls, etc., or if the plot was oriented differently). To facilitate scan registration,
 298 all tilt scans along the first sampling line were oriented towards the same sampling position along the next sampling line, and
 299 all other tilt scans along plot edges were oriented towards the inside of the plot so that the previous scan location was within
 300 the tilt-scan field of view. Depending on the density of the canopy understory, terrain, and wind conditions (ideally, low to
 301 zero wind and no rain or mist/fog), a team of three experienced TLS operators required 1–2 full working days (8 hrs per day)
 302 to set up the chain sampling grid and 3–5 full days to complete the scanning of a 1 ha plot.

304 TLS data for all three FBRMS were collected using a RIEGL VZ-400 laser scanner or its newer model, the VZ-400i, which
 305 has very similar technical specifications (see Table 1) and includes Global Navigation Satellite System (GNSS) Real-Time
 306 Kinematic (RTK) positioning (RIEGL Laser Measurement Systems GmbH, 2025). RTK GNSS facilitates TLS data acquisition
 307 by replacing the labour-intensive and time-consuming task of placing and continuously relocating retro-reflective targets
 308 between scan positions as required by the RIEGL VZ-400 scanner. Common targets between adjacent scan locations were
 309 later identified and used to create a registration chain that integrates the 3D point cloud of a scanned plot. GNSS RTK has
 310 replaced the use of common targets, enabling the absolute (latitude, longitude, and altitude) and relative (between base and
 311 rover GNSS) positioning of individual scans with centimetre precision, which makes the auto-registration of scans in real-time
 312 possible. This GNSS-enabled auto-registration significantly reduces the time and effort required to both collect and register
 313 TLS data. Furthermore, data collected with the VZ-400i are backwards compatible with data from the older VZ-400 scanner,
 314 allowing for consistent processing and comparison over time.

315

316 **Table 1:** Characteristics of RIEGL laser scanners (RIEGL Laser Measurement Systems GmbH, 2025) used for TLS data
 317 acquisition at ForestScan FBRMS.

Characteristic	RIEGL VZ-400	RIEGL VZ-400i
Max Pulse Repetition Rate [kHz]	300 – 1200 (300 used)	300 – 1200 (300 used)
Angular resolution	0.04° (22.4 million emitted pulses per scan, i.e. 5.42 billion per hectare)	0.04° with 22.4 million emitted pulses per scan (5.42 billion per hectare)
Wavelength [nm]	~1550 (near-infrared)	~1550 (near-infrared)
FOV [°]	360 (horizontal)	360 (horizontal)
Ranging accuracy / precision [mm]	5 / 3	5 / 3
Max range [m]	~800 @ 80% reflectivity	~800 @ 80% reflectivity
Beam divergence [mrad]	0.35	0.35
Beam diameter at emission [mm]	7	7
Returns per pulse	Up to 7	Unlimited (waveform)
Scan time per scan	3 minutes	3 minutes
GNSS RTK positioning	No	Yes (integrated)
Weight [kg]	~13	~13
Operated by	UCL	UCL

Scan site (s)	FBRMS-03: Malaysia	FBRMS-01: French Guiana FBRMS-01: Gabon
---------------	--------------------	--

318

319 **TLS: FBRMS-01: Paracou, French Guiana**

320 TLS data was collected in Paracou over two separate periods due to interruptions caused by the COVID-19 pandemic. The
321 first campaign took place in 2019, censused plot FG6c2 was scanned with a RIEGL VZ-400 scanner during October and
322 November (Brede et al., 2022a). The scanning was conducted over a 200 x 200 m² area (i.e. two 1 ha plots) covering two of
323 plot 6 subplots -2 and 4- (see Panel c in Fig. 1), resulting in 21 x 21 scan lines with 10 m grid spacing. Retro-reflective targets
324 were placed between scan positions to facilitate coarse registration (Wilkes et al., 2017).

325

326 The second TLS campaign took place in 2022, three 1 ha censused plots (see Fig. 1) were scanned during September and
327 October using a RIEGL VZ-400i scanner with GNSS RTK-enabled auto-registration. These plots were selected to represent
328 the disturbance gradient found at this site, as shown in Table 2. All three plots were also scanned with ALS and plot FG6c2
329 additionally scanned with UAV-LS.

330

331 **Table 2:** Overview of plots scanned in 2022 with TLS in Paracou, French Guiana.

Plot ID	Subplot	Logging treatment	Description	AGB	Lat	Long
FG6c2	2	Control	Old-growth, lowland, Terra firme rainforest	High	5.27	-52.92
FG5c1	1	T2	Old-growth, lowland, Terra firme rainforest with mid-level logging disturbance	Mid	5.27	-52.92
FG8c4	4	T3	Old-growth, lowland, Terra firme rainforest with high-level of logging disturbance	Low	5.26	-52.93

332

333 **TLS: FBRMS-02: Lopé, Gabon**

334 TLS data was collected in 2022, four 1 ha plots were scanned using a RIEGL VZ-400i with GNSS RTK-enabled auto-
335 registration, eliminating the need for retro-reflective targets between scan positions. The four sampled plots, shown in Table
336 3, were selected to represent the diversity of forest types found within this site.

337

338 **Table 3:** Overview of plots scanned with TLS in Lopé National Park, Gabon.

Plot ID	Description (local plot name / forest type)	Lat	Long
LNL-07	OKO-01 / Maturing secondary Okoumé forest	-0.19	11.58
LNL-08	OKO-02 / Maturing secondary Okoumé-Sacoglottis forest	-0.19	11.58
LNL-09	OKO-03 / Maturing secondary Okoumé forest	-0.19	11.57
LPG-01	Angak / Old-growth forest	-0.17	11.57

339

340 **TLS: FBRMS-03: Kabili-Sepilok, Malaysian Borneo**

341 TLS data was collected for three 1 ha forest plots at this FBRMS during March 2017. The three sampled plots, shown in Table
 342 4, were selected to represent the three distinct forest types found within this site. A RIEGL VZ-400 scanner was used, with
 343 retro-reflective targets positioned between scan locations to facilitate coarse registration (Wilkes et al., 2017).

344

345 **Table 4:** Overview of plots scanned with TLS in Kabili-Sepilok Forest Reserve, Malaysia. Note: subplot 2 was

Plot ID	Subplot	Description (local plot name / forest type)	Lat	Long
SEP-11	2	292/3 / Sandstone forest	5.86	117.94
SEP-12	2	292/1 / Alluvial forest	5.86	117.93
SEP-30	3	508/4 / Kerangas forest	5.86	117.97

346

347 **TLS data processing**

348 TLS data was collected and processed to provide state-of-the-art estimates of tree- and plot-scale structural attributes and AGB
 349 for each ForestScan FBRMS. Five main processing steps are required to retrieve structural attributes from the acquired TLS
 350 data are described below. These processing steps demand significant computational resources -a full 1 ha plot can take 3.4 to
 351 4 days to process from start to finish on a high performance computing (HPC) cluster, running on multiple central processing
 352 units (CPUs; general-purpose processors optimised for sequential tasks and complex logic) and graphics processing units
 353 (GPUs; highly parallel processors ideal for deep learning, point cloud processing and simulations tasks that can be broken into
 354 thousands of simultaneous operations).

355

356 **1. Individual scan registration into plot-level point cloud**

357 This process was carried out using retro-reflective targets positioned between scan locations to facilitate coarse registration for
358 data collected with the RIEGL VZ-400 or in a near-automated manner using the RIEGL VZ-400i's GNSS RTK positioning
359 capabilities in conjunction with the enhanced RIEGL RiSCAN Pro software (versions 2.14–2.17). The integrated Auto
360 Registration 2 (AR2) function employs GNSS RTK data to update the scanner's position and orientation, including in tilt
361 mode, thereby enabling real-time automated coarse registration during scanning. Major registration errors are easily detected,
362 typically occurring during pre-processing in RiSCAN Pro when individual scans fail to register (i.e., no coherent solution is
363 found) or are incorrectly positioned, which is visually apparent. In cases where coarse registration/auto-registration fails,
364 unregistered scans can be identified, adjusted, and refined using Multi Station Adjustment 2 (MSA2). Following this workflow,
365 the co-registration of all TLS point clouds achieves sub-centimetre accuracy, as confirmed through post-registration inspection.
366 Wind and occlusion are key sources of uncertainty for the scan registration process, highlighting the necessity of scanning
367 under low or zero wind conditions and capturing both tilt and upright scans at each location.

368

369 The use of GNSS significantly enhances the utility and accessibility of TLS by drastically reducing both data acquisition and
370 processing time. This is achieved by (1) as previously mentioned, replacing the previous labour-intensive and time-consuming
371 practice of using common retro-reflective targets to link adjacent scan positions into a registration chain (Wilkes et al., 2017),
372 and (2) reducing the manual processing registration time by an experienced user to 1 - 2 days per hectare, which is less than
373 half the time required when using retro-reflective targets.

374

375 Registration results in a plot-level point cloud, comprising 242 individual scan-level point clouds, potentially containing more
376 than 5.42 billion points.

377

378 The subsequent four processing steps were performed in a semi-automated manner using the *rxp-pipeline* (Wilkes and Yang,
379 2025a) and *TLS2trees* processing pipelines (Wilkes et al., 2023) and *TreeQSM* version 2.3 (Raumonen et al., 2013), as
380 described below.

381 **2. Pre-processing of plot-level point clouds**

382 Pre-processing is carried out in three steps using the open-source tool *rxp-pipeline* (Wilkes and Yang, 2025a), which operates
383 directly on the raw RIEGL scan data. First, the co-registered RIEGL point clouds are filtered to remove points with a deviation
384 greater than 15 and reflectance outside the range [-20, 5]. The data are then clipped to the plot extent, with an additional 10 m
385 around the plot, segmented into 10 m x 10 m tiles, and converted from the RIEGL proprietary .rxp to .ply format to enable
386 further processing. Second, to reduce computing load, the tiled point clouds are downsampled using a voxelisation approach
387 with a voxel size of 0.02 m, implemented via *PDAL VoxelCenterNearestNeighbor* filter (PDAL Contributors, 2025). Finally,

388 a tile index mapping the spatial location of each tile is generated. In a HPC system, preprocessing of a 1 ha plot can take 1.58
389 to 4.17 hours to complete.

390 **3. Semantic segmentation: wood-leaf separation**

391 *TLS2trees* is an open-source Python command-line pipeline (Wilkes et al., 2025) designed to automate tree extraction from
392 TLS point clouds by utilising GPUs for parallel computation, making it fully scalable on HPC systems (Wilkes et al., 2023).
393 The first of the two-step *TLS2trees* workflow employs a deep-learning based approach, implementing a modified version of
394 the Forest Structural Complexity Tool (FSCT) semantic segmentation method by Krisanski et al. (2021) to classify points
395 within tiled point clouds into homogeneous classes representing distinct biophysical components: leaf, wood, coarse woody
396 debris, or ground. An example of the wood and leaf classes extracted from tree-level point clouds is illustrated in Fig. 5. In a
397 HPC system, semantic segmentation of a 1 ha plot can take 4 to 12 hours to complete.
398



399
400 **Figure 5:** Tree-level point cloud of the largest *Baillonella toxisperma* (Maobi) tree (~40 m tall with an almost circular
401 canopy ~50 m wide) in plot LPG-01, FBRMS-02: Lopé, Gabon. Points are classified and displayed by category only: wood
402 points in brown and leaf points in green.

403 **4. Instance segmentation: individual tree separation**

404 The second step in the *TLS2trees* workflow identifies and segments individual trees via a 2-step process. The Dijkstra's shortest
405 path method first groups all points identified as wood into a set of individual woody stems to which points identified as leaf
406 are then assigned. A small group of trees automatically segmented from a plot in Gabon are shown in Fig. 6. In a HPC system,
407 instance segmentation of a 1 ha plot can take 15-20 hours to complete.
408



409 **Figure 6:** Individual tree-level point clouds acquired from plot LPG-01 in FBRMS-02: Lopé, Gabon.

410 **5. TreeQSM: quantitative structural models and results**

411 Quantitative structural models (QSMs) were constructed in a near-automated manner from each individually segmented tree
412 point cloud (woody components only) with a DBH ≥ 10 cm within each ForestScan FBRMS plot. This was achieved using the
413 *TreeQSM* software package (version 2.3; Raumonen et al., 2013), which reconstructs underlying woody surfaces by fitting
414 cylinders, as illustrated in Fig. 7. The QSM fitting process involves three steps: (i) reducing each point cloud to a series of
415 patches, (ii) analysing the spatial arrangement and neighbour relationships among patches, and (iii) robustly fitting cylinders
416 to common patches.

417

418 The overall QSM fit is controlled by three parameters, which are iterated into 125 different parameter sets, each generating
419 five models. This yields a total of 625 candidate models per segmented tree. The optimal model is then selected by minimising
420 the point-to-cylinder surface distance (Burt et al., 2019; Martin-Ducup et al., 2021). Estimates of morphological and
421 topological traits such as volume, length, and surface area metrics, along with their mean and standard deviation, are derived

422 from the five models that share the same parameters as the optimal model. This approach provides an estimate of the
423 uncertainty associated with the resulting volume (Wilkes et al., 2023). In a HPC system, QSMs for a 1 ha plot can take up to
424 2 days to complete.

425

426



427

428 **Figure 7:** QSMs derived from individual tree-level point clouds acquired from plot LPG-01 in FBRMS-02: Lopé, Gabon.

429

430 Uncertainty estimates are reported for each ForestScan FBRMS plot and included alongside the final modelling outputs for
431 every tree in a ‘tree-attributes.csv’ file, generated at the end of the modelling process. Sources of error in QSM fitting can arise
432 from data acquisition (e.g., wind, leaf occlusion, understory vegetation) and from assumptions inherent in segmentation and
433 fitting processes. Wilkes et al. (2017) discuss issues related to data acquisition and methodological choices, while Morhart et
434 al. (2024) quantify their effects on branch size and volume under controlled conditions. Although these impacts are difficult
435 to assess without reference (harvest) data, Demol et al. (2022) show that, where TLS and harvest data have been compared,
436 agreement is generally within a few percent of AGB per tree. The report CVS file also includes tree- and plot-level carbon and

437 AGB estimates, the latter based on a mean pantropical wood density value of 0.5 g cm⁻³ derived from the DRYAD global
438 database of tropical forest wood density (2009). Plot-level AGB was also estimated using DRYAD-derived regional mean
439 wood densities and is presented in Table 5.

440
441 Figures of all individually segmented trees arranged by tree DBH size (largest to smallest DBH) are also generated for each
442 FBRMS plot, examples of which can be seen in Fig. 8. In a HPC system, tree figure for a 1 ha plot can take ~30 mins to
443 complete. Figure 9 provides a comparison of the distribution of DBH measurements collected by tree census and TLS methods
444 at each of the 10 ForestScan FBRMS 1 ha plots.

445 **TLS datasets**

446 The following terrestrial LiDAR-derived products are available for each of the 10 ForestScan FBRMS plots:

- 447 1. Raw terrestrial LiDAR data from each scan (no filtering was applied in RiSCAN PRO), stored in the RXP data stream
448 format developed by RIEGL.
- 449 2. Transformation matrices necessary for rotating and translating the coordinate system of each scan, into the coordinate
450 system of the first scan. Stored in DAT format.
- 451 3. Pre-processed terrestrial LiDAR data:
 - 452 a. full-resolution 10m tiled plot point clouds including attributes such as XYZ, scan position index, reflectance,
453 deviation, etc. stored in polygon PLY format.
 - 454 b. downsampled 10m tiled plot point clouds including attributes such as XYZ, scan position index, reflectance,
455 deviation, etc. stored in polygon PLY format.
 - 456 c. A tile_index file (maps the spatial location of the tiled point clouds) stored in DAT format.
 - 457 d. Bounding geometry files setting plot boundaries with and without a buffer surrounding the plot. Stored in
458 shapefile SHP, DBF, SHX and CPG formats.
- 459 4. Downsampled 10m tiled plot point clouds segmented into leaf, wood, ground points or coarse woody debris. Stored
460 in polygon file format PLY format.
- 461 5. Wood-leaf separated tree-level point clouds including **segmentation results and classification probabilities** for each
462 point are stored in polygon PLY format.
- 463 6. QSM files:
 - 464 a. **in_plot** CSV (for plots processed with *TLS2trees*) lists all trees to be modelled with QSMs as they are located
465 inside the plot boundary.
 - 466 b. **out_plot** CSV (for plots processed with *TLS2trees*) lists all trees NOT to be modelled as they are located
467 outside the plot boundary.
 - 468 c. **plot_boundary** CSV (for plots processed with *TLS2trees*) shows the location of all in_plot trees within each
469 plot boundary.

- d. **QSM processing files** (.MAT Matlab).
- e. **QSMs** derived from each woody tree-level point cloud, (.MAT Matlab).

7. We provide pre-processed and segmented terrestrial LiDAR data in PLY format as it supports full 3D object representation, including polygons and geometric primitives, in addition to point data. This is essential for storing quantitative structure models (QSMs), which go beyond point clouds to describe tree geometry. The PLY format is open, widely supported in Python and R, and can be converted to LAS/LAZ when only point data are required.

8. Tree-attributes file (.CSV) containing biophysical parameters derived from both the point clouds and QSMs: DBH, tree height, tree-level volume and AGB with uncertainty, plot-level AGB and associated uncertainty.

9. Figures of all individually segmented trees arranged by tree DBH size (largest to smallest DBH) for each FBRMS plot (see Fig. 8) (PNG image format).

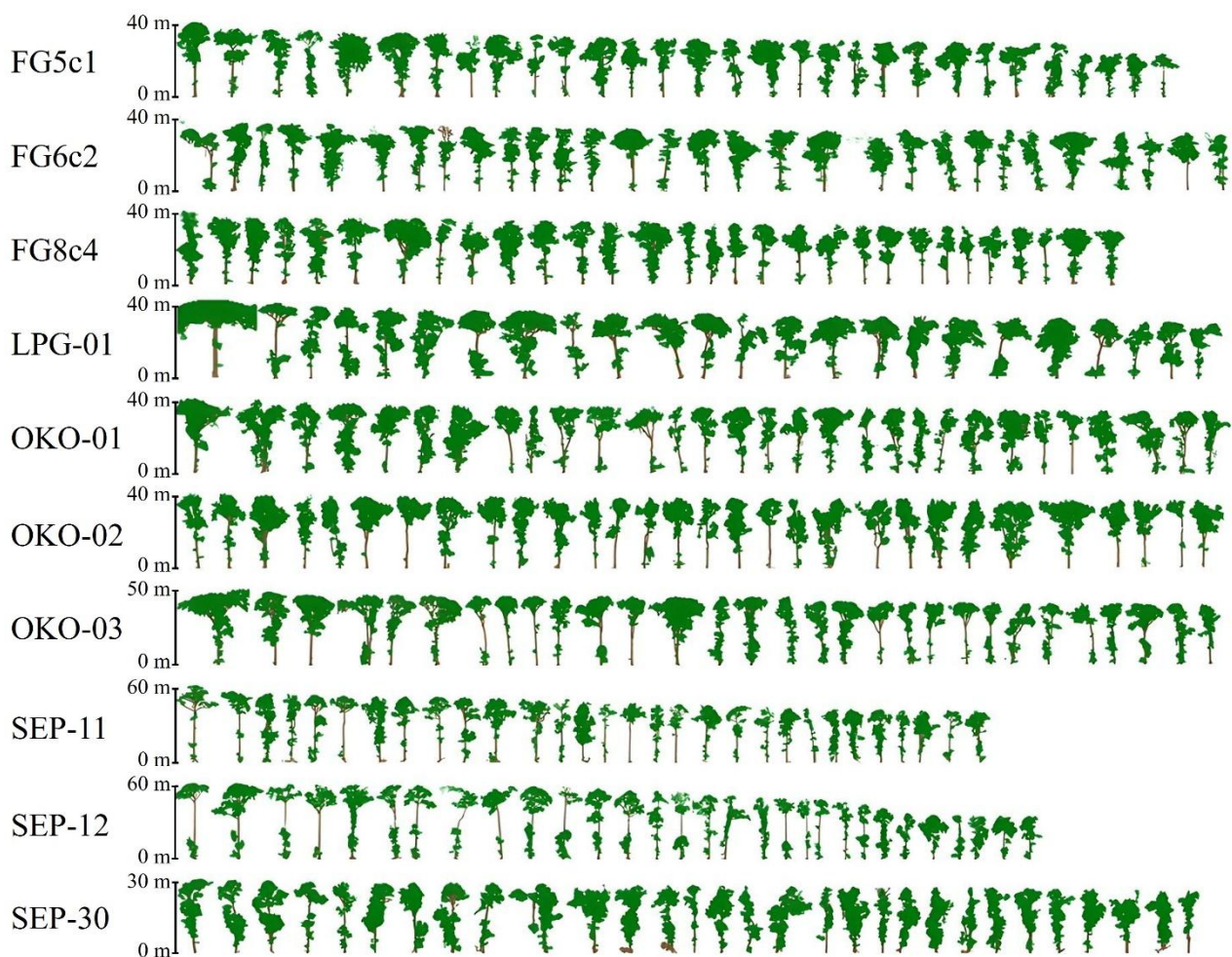
10. GNSS coordinates (geographical coordinate system: WGS84 Cartesian) for all scan positions stored in KMZ zip-compressed format. These files are available for the seven French Guiana and Gabon FBRMS plots.

These TLS ForestScan FBRMS 1 ha plot datasets are freely available via the Centre for Environmental Data Analysis (CEDA) with URLs and DOIs provided in section 5.

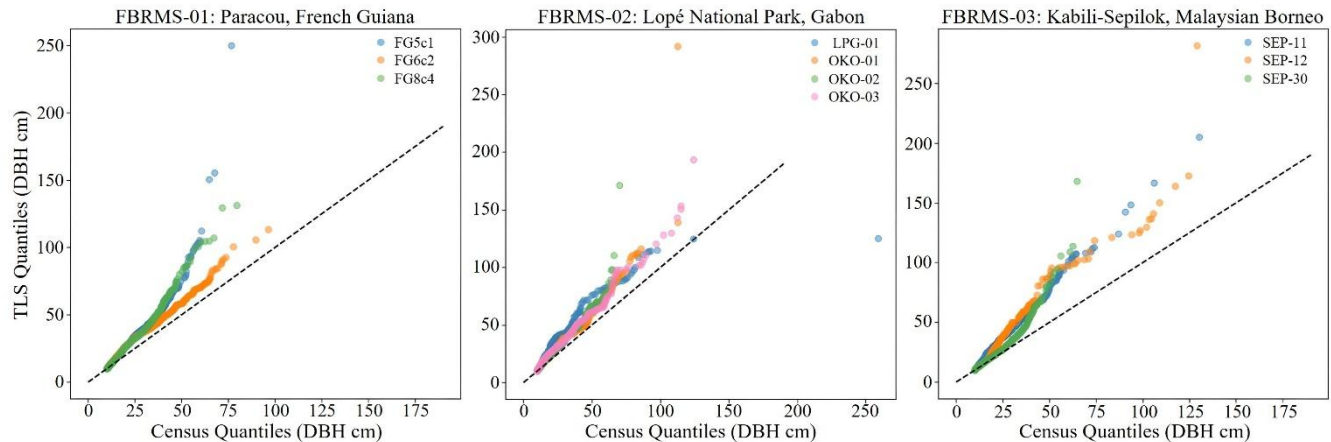
QSMs can be converted to PLY format using open-source tools such as *mat2ply* (Wilkes and Yang, 2025b) and then read by various tools such as the widely-used free GUI tool CloudCompare (CloudCompare Development Team, 2025; <https://www.cloudcompare.org>), via Python using PDAL (PDAL Contributors, 2025; <https://zenodo.org/records/4031609>) or O3d (Open3D Development Team, 2025; https://www.open3d.org/docs/0.9.0/tutorial/Basic/file_io.html#mesh), or via the R Geomorph package (Adams et al., 2025; <https://rdrr.io/cran/geomorph/man/read.ply.html>). In the Geomorph R package, the function `Read mesh data (vertices and faces)` from PLY files can be used to read three-dimensional surface data in the form of a single PLY file (Polygon File Format; ASCII format, from 3D scanners). Vertices of the surface may then be used to digitise three-dimensional points. The surface may also be used as a mesh for visualising 3D deformations using the `warpRefMesh` function. The function opens the PLY file and plots the mesh, with faces rendered if file contains faces, and coloured if the file contains vertex colour. Vertex normals allow better visualisation and more accurate digitising with `digit.fixed`. The KMZ files containing the GNSS scan position coordinates can be uploaded to Google Earth or read into a GIS tool such as QGIS (QGIS Development Team, 2025; <https://qgis.org>).

Table 5: Summary statistics for 10 FBRMS ForestScan TLS plot datasets. AGB estimates use wood density values from the DRYAD global database (Zanne et al., 2009): (1) *TLS2Trees* pantropical mean, (2) Tropical Africa mean (TAF, Gabon), (3) South-East Asia mean (TS-EA, Malaysia), (4) Tropical South America mean (TSA, French Guiana), (5) Guyana community mean (GF, French Guiana), and (6) allometric AGB estimates based on Chave et al. (2014).

Plot ID	Site	Cens us trees (≥ 10 cm DB H)	TLS2trees plot summary				TLS2trees Carbon estimation		TLS2trees AGB estimations (1)				Tropical Africa (TAF; 2) / Tropical South America (TSA; 4) / Tropical South-East Asia (TS-EA; 3) AGB estimations			Guyana AGB estimations (5)			2014 Allom etric AGB estima tion (6)
			TLS trees (#)	TLS vs Census trees (%)	TLS plot area (ha)	TLS plot volum e (m ³)	Plot C (t)	C per ha (t/ha)	Wood density (g/cm ³)	Plot AGB (t)	AGB per ha (t/ha)	Wood density (g/cm ³)	Plot AGB (t)	AGB per ha (t/ha)	Wood density (g/cm ³)	Plot AG B (t)	AGB per ha (t/ha)	Plot AGB (t)	
OKO-01	GA	388	397	2.58	1.08	829.05	195.24	181.60	0.5	414.52	385.57	0.60	495.77	459.05				378.62	
OKO-02	GA	472	473	0.21	1.02	625.45	147.29	143.97	0.5	312.72	305.67	0.60	374.02	366.69				351.35	
OKO-03	GA	339	355	4.72	1.04	959.59	225.98	218.19	0.5	479.79	463.26	0.60	573.83	551.76				372.82	
LPG-01	GA	340	275	-19.12	1.05	477.88	112.54	107.16	0.5	238.94	227.52	0.60	285.77	272.17				459.85	
FG5c_1	GF	1110	804	-27.57	1.06	529.67	124.74	117.62	0.5	264.83	249.73	0.63	334.75	315.80	0.73	386. 66	409.86	327.30	
FG6c_2	GF	902	832	-7.76	1.10	751.13	176.89	161.48	0.5	375.57	342.86	0.63	474.72	431.56	0.73	548. 33	603.16	421.90	
FG8c_4	GF	1116	1090	-2.33	1.09	625.80	147.38	135.76	0.5	312.90	288.24	0.63	395.50	362.85	0.73	456. 83	497.95	286.10	
SEP-11	MY	584	659	12.84	1.05	961.36	226.40	214.67	0.5	480.68	455.78	0.57	551.82	579.41				499.91	
SEP-12	MY	469	380	-18.99	1.13	765.51	180.28	158.98	0.5	382.76	337.53	0.57	439.40	496.53				443.45	
SEP-30	MY	787	986	25.29	1.03	374.66	88.23	85.25	0.5	187.33	181.01	0.57	215.05	221.50				311.54	



506 **Figure 8:** Examples of the largest trees (up to 30 trees) arranged in decreasing DBH size (1.3 m trunk height) for each of the
507 10 ForestScan FBRMS plots. The upper limit of the Y axis varies and ranges from 30 m to 60 m maximum tree size between
508 plots.



509
510 **Figure 9:** Quantile-Quantile (QQ) plots comparing the distribution of DBH measurements collected by tree census and TLS
511 methods at each of the 10 ForestScan FBRMS 1 ha plots. TreeQSM measures DBH at the standard height of 1.3 m for each
512 TLS-extracted tree, whereas census DBH measurements are routinely adapted to account for tree buttresses found among
513 larger trees. Generally, census and TLS DBH measurements are in good agreement but consistently overestimated by TLS.
514 Deviations for larger DBH values can be improved by adapting the DBH extraction of large buttressed trees once these trees
515 are matched to their census counterparts. The 1:1 reference line (dotted black line) represents perfect agreement between
516 census and TLS-extracted DBH measurements.

517 **2.2.3 Unpiloted Aerial Vehicle laser scanning (UAV-LS)**

518 Unlike TLS, there are currently no best practice guidelines for UAV-LS data acquisition for forest characterisation. Therefore,
519 flight plans and parameters were implemented on a case-by-case basis, considering the site, instrument, sensor, and application.
520 An important consideration in this respect is whether VLOS needs to be maintained, i.e., the visibility of the platform by the
521 pilot throughout the mission. Regulations on this vary nationally and are changing rapidly as technology evolves and the use
522 of UAVs expands. In Europe, for example, a risk-based approach has been introduced, allowing beyond VLOS when risks are
523 negligible.

524

525 Another important consideration is the availability of take-off and landing areas. Vertical take-off and landing (VTOL)
526 platforms (e.g., quadcopters and octocopters) require smaller areas and are more flexible, while fixed-wing platforms may
527 require substantial take-off and landing sites, although they offer greater area coverage and flight duration. The actual take-off
528 area for VTOL platforms is highly dependent on the skills and confidence of the pilot. However, a very small take-off area
529 surrounded by tree crowns typically also means low chances for VLOS operation, unless an above-canopy platform such as a
530 cherry-picker is available.

531

532 In the context of VTOL and VLOS operations, viewshed analysis based on already acquired ALS data has proved useful. ALS
533 point clouds can be used to derive initial Digital Surface Models (DSM), which can identify possible take-off positions.
534 Viewshed analysis can then use the DSM to simulate the visibility of the UAV from the take-off position.

535

536 During data collection, attention should also be paid to acquiring access to GNSS observables from permanent base stations
537 (e.g., CORS network) or to collecting observables with a temporary base station (e.g., Emlid Reach RS+ or RS2). A base
538 station should be positioned less than 15 km from the survey area. For some platforms, Real-Time Kinematic (RTK), and
539 therefore radio connection, between the UAV and base station can be an added constraint.

540

541 Our UAV-LS data collections used three different LiDAR systems built by RIEGL at FBRMS-01 and FBRMS-02. All systems
542 are based on the time-of-flight principle and capable of multi-return registration with the miniVUX-1DL being a specific
543 downward-looking sensor designed for fixed-wing UAVs. Technical specifications for all three UAV-LS sensor systems are
544 provided in Table 6.

545

546 **Table 6:** UAV-LS sensor systems used at ForestScan FBRMS-01 and FBRMS-02.

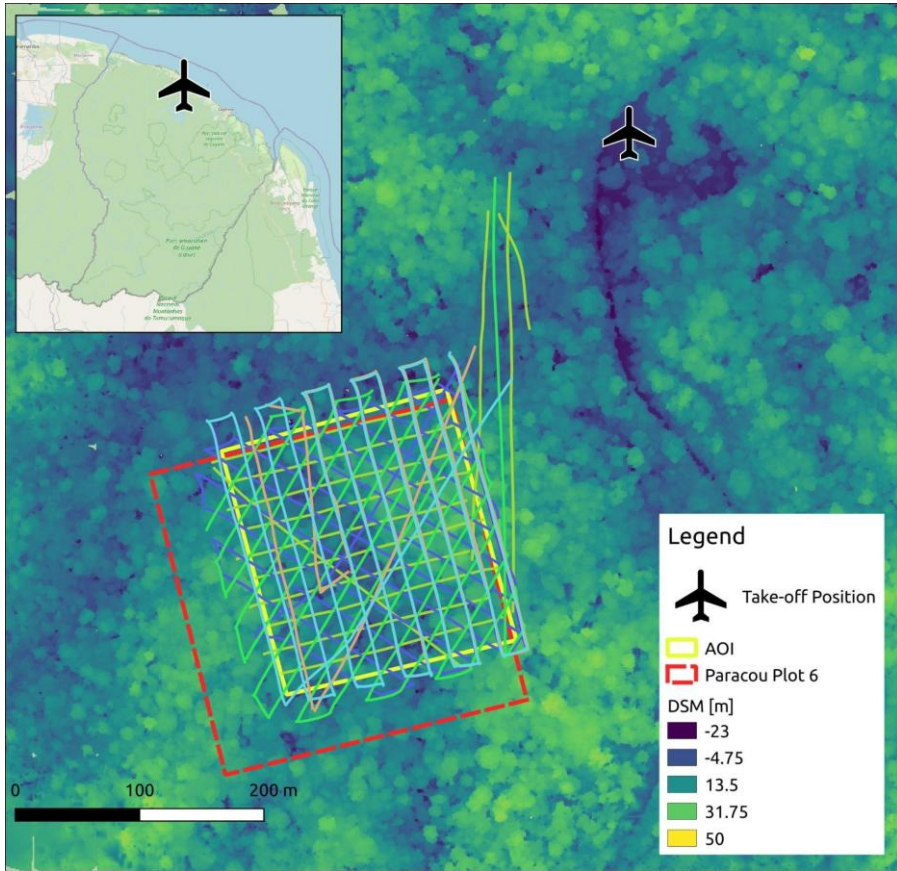
Characteristic	miniVUX-1UAV	VUX-1UAV	miniVUX-1DL
Max Pulse Repetition Rate [kHz]	100	550	100

Wavelength [nm]	905	1550	905
FOV [°]	360	330	46
Ranging accuracy / precision [mm]	15 / 10	10 / 5	15 / 10
Max range [m]	330 @ $\rho \geq 80\%$	1050 @ $\rho \geq 80\%$	260 @ $\rho \geq 80\%$
Weight [kg]	1.55	3.5	2.4
Inertial Measurement Unit (IMU)	Applanix APX20	Applanix AP20	Applanix APX15
Operated by	AMAP	Wageningen University	University of Edinburgh
Operated on	DJI M600	RiCOPTER	DELAIR DT26X
Flight location	FBRMS-01: Paracou	FBRMS-01: Paracou	FBRMS-02: Lopé
Flights merged into single acquisition	No	No	Yes

547

548 **UAV-LS: FBRMS-01: Paracou, French Guiana**

549 UAV-LS data was collected in October 2019 using two different scanning systems as shown in Tables 7 and 8. The first set
 550 of 11 flights listed in Table 7 were conducted using the RIEGL VUX-1UAV mounted on a RIEGL RiCOPTER UAV and
 551 flown over the same 200 x 200 m² area that was scanned with TLS covering subplots 2 and 4 in plot 6. Six of these flights
 552 covered the entire 200 x 200 m² area with 20 m spacing between flight lines at an altitude of 120 m above ground level (AGL).
 553 The remaining five flights covered only the north-east 100 x 100 m² area covering subplot 2 (i.e. FG6c2) with a criss-cross
 554 pattern to maximise the diversity of viewing angles into the canopy. These latter flights were conducted at a lower altitude of
 555 90 m AGL to increase point density; however, the entire plot could not be covered without losing VLOS.
 556



557

558 **Figure 10:** UAV-LS flight trajectories over the FBRMS-01 site at Paracou, showing coverage of the experimental 4 ha plot 6
 559 (red dashed outline) and the area of interest (AOI; yellow dashed outline). The criss-cross flight pattern results from multiple
 560 flight lines oriented in different directions (e.g., N–S, E–W, NE–SW) to improve point density and reduce occlusion in dense
 561 tropical forest canopies. The background shows a digital surface model (DSM) with elevation values (m), colour-coded by
 562 elevation classes as indicated in the figure legend (–23 m to 50 m). The inset map shows the regional location of Paracou
 563 within French Guiana (© OpenStreetMap contributors, available at <https://www.openstreetmap.org>).
 564

565 **Table 7:** Overview of the 2019 VUX-1 UAV-LS flights at FBRMS-01 (Paracou), including plot ID, acquisition date/time,
 566 flight height above ground level (AGL), speed, and pulse repetition rate. Flight patterns refer to the orientation of flight lines:
 567 N–S (north–south), E–W (east–west), NE–SW (northeast–southwest), and “criss-cross” indicates multiple orientations flown
 568 over the same area as seen in Fig. 10. All flights listed can be considered part of one acquisition and are provided as individual
 569 point clouds in this dataset. Users may merge them according to their needs.

Plot ID	Date & Time (UTC ISO 8601)	Direction [°]	Interline [m]	Alt	Speed [m/s]	Pulse Repetition Rate [kHz]
---------	-------------------------------	---------------	------------------	-----	----------------	--------------------------------

				AGL [m]		
P6 200	2019-10-18T11:41:05Z	Manual	20	115	4	550
P6 200	2019-10-18T13:28:27Z	165	20	110	6	550
P6 200	2019-10-18T14:36:54Z	75	20	105	7	550
P6 200	2019-10-18T175:7:53Z	120	20	115	6	550
P6 200	2019-10-18T19:23:14Z	30	20	105	6	550
P6 200	2019-10-19T16:34:12Z	165	20	120	6	300
P6 200	2019-10-20T18:45:40Z	165	20	120	6	100
P6 100	2019-10-19T12:10:41Z	multiple headings	variable	95	4	550
P6 100	2019-10-19T12:41:09Z	multiple headings	variable	85	4	550
P6 100	2019-10-19T18:19:57Z	multiple headings	variable	95	4	550
P6 100	2019-10-19T19:41:42Z	multiple headings	variable	90	4	550

570

571 UAV-LS data was also collected over several plots using a different UAV-LS system -a YellowScan Vx20 containing a RIEGL
 572 Mini-VUX scanner and Applanix 20 IMU- mounted on a DJI M600. Details for a second set of 12 flights can be found in
 573 Table 8. To allow for comparisons with the VUX system, coincident acquisitions were performed over experimental plot 6
 574 (covering all four subplots) and several others within the Paracou Research Site (see Table 8).. A full description of the UAV-
 575 LS data collection for this UAV-LS data is provided in Brede et al. (2022b).
 576

577 **Table 8:** Overview of UAV-LS flights using a YellowScan Vx20 system (RIEGL Mini-VUX scanner and Applanix 20 IMU)
 578 mounted on a DJI M600 during the 2019 mission at the FBRMS-01 site. Automated flight plans were performed using flight
 579 plans with the UgCS route planning software in grid mode. The table lists plot ID, acquisition date/time, flight parameters
 580 (direction, interline spacing, altitude and speed). Altitude values are reported as specified during flight planning with some
 581 missions using Above Ground Level (AGL), while others used Above Mean Sea Level (AMSL) due to differences in mission
 582 planning and operational requirements. These original specifications are retained to accurately reflect acquisition parameters.
 583 Pulse repetition for the RIEGL Mini-VUX scanner is fixed at 100kHz. Flights cover multiple experimental plots: 4 & 5 (single
 584 flight), 6 (8 flights), 7, 8, 10, 15, and the Tower plot (two flights) within the Paracou Research Site. All listed flights are
 585 provided individually; users may merge flights covering the same plot if needed for analysis.

Plot ID	Date & Time (UTC)	Direction [°]	Interline [m]	Alt [m]	Speed [m/s]	Pulse Repetition Rate [kHz]
P4 & P5	2019-10-19T17:23:47Z	345	50	100 amsl	5	100
P6	2019-10-18T12:40:06Z	345	20	80 AGL	5	100
P6	2019-10-18T13:10:43Z	345	20	80 AGL	5	100
P6	2019-10-18T18:30:57Z	120	20	80 AGL	5	100
P6	2019-10-18T18:54:16Z	120	20	80 AGL	5	100
P6	2019-10-18T20:09:32Z	165	20	145 amsl	5	100
P6	2019-10-19T11:59:17Z	75	20	145 amsl	5	100
P6	2019-10-19T19:03:45Z	75	20	80 AGL	5	100
P6	2019-10-20T19:17:57Z	345	40	100 amsl	3	100
P8	2019-10-20T11:39:07Z	75 & 345	50	105 amsl	5	100
P GuyaFlux tower/CNES (tropiscat)	2019-10-19T16:25:57Z	0	50	80 AGL	5	100
P GuyaFlux tower/CNES (tropiscat)	2019-10-19T18:10:21Z	90	50	105 amsl	5	100

586

587 **UAV-LS data processing**

588 All collected raw data underwent processing with standard tools. For VUX-1UAV data, this included processing
 589 recorded [global navigation satellite system](#) (GNSS) and base station data to flight trajectories with POSPac [Mobile](#)
 590 [Mapping](#) Suite 8.3 (Applanix, Richmond Hill, Ontario, Canada), laser waveform processing to discrete returns and geolocation
 591 in world coordinates with RIEGL RiProcess 1.8.6. For miniVUX-1UAV, waveform processing is performed online in the
 592 sensor. Point cloud processing and geolocation was performed with the CloudStation software (YellowScan, Montpellier,
 593 France), using the Strip Adjustment option. For all UAV-LS data, only points with a reflectance larger than -20 dB were kept
 594 for further processing. Points with reflectance smaller than -20 dB consist mainly of spurious points caused by water droplets
 595 under high humidity conditions ([Schneider et al., 2019](#)).

596

597 LiDAR point clouds were processed using the *LASTools* suite (rapidlasso GmbH). First, a 1-m resolution digital surface model
598 (DSM) was generated with **lasgrid** using the highest return within each cell. Ground points were then classified
599 with **lasground** (wilderness settings, 15-m step), and a 1-m digital terrain model (DTM) was derived from ground-classified
600 points using **las2dem**. Heights were normalized by subtracting ground elevation with **lasheight**, producing a set of height-
601 normalized point clouds. A 1-m canopy height model (CHM) was computed with **lascanopy**, retaining the maximum height
602 in each grid cell after removing noise and low-confidence classes. Finally, a point density map (1-m resolution) was created
603 using **lasgrid** with the *counter* option. This workflow produced consistent DSM, DTM, CHM, and density layers suitable for
604 subsequent ecological analyses. These UAV-LS datasets are freely available via the Centre for Environmental Data Analysis
605 (CEDA) with DOIs provided in section 5. Data access.

606 **UAV-LS: FBRMS-02: Lopé, Gabon**

607 UAV-LS data was collected in June 2022, concurrently with TLS data acquisition at this FBRMS. Data was acquired using a
608 DELAIR DT26X drone platform equipped with a RIEGL miniVUX-1DL (Mcnicol et al., 2021) as seen in Fig. 11. This
609 platform differs from the one used at FBRMS-01: Paracou in that it is designed for large-scale data acquisitions (thousands of
610 hectares) and is capable of operating beyond the VLOS, with an average flight speed of 17 m/s (61 km/h). Flights were
611 conducted in perpendicular lines at a nominal altitude of 120 m above the ground surface, with an average flight line spacing
612 of 20 m (based on 70–80% overlap). Each one-hour flight covered approximately 120–200 hectares with an estimated point
613 density of 400 points per square metre. To obtain the required densities, several flights were conducted over the core plots
614 from different angles (depending on wind conditions) to maximise the diversity of viewing angles into the canopy.

615



616

617

618 **Figure 11:** UAV-LS acquisitions at FBRMS-02: Lopé using a fixed-wing system. This UAV employs a conventional take-off
 619 and landing (CTOL) procedure, with launch aided by a catapult (top). Once airborne, the UAV is controlled from a laptop
 620 connected to the UAV via an antenna (middle). The flight trajectory is corrected to centimetre precision using data collected
 621 from a static GNSS receiver placed within 10 km of the UAV operating area (lower left). Additional refinements and
 622 corrections are possible via ground control points located across the study area (lower middle), the positions of which are
 measured using a 'rover' GNSS receiver (lower right). Image originally published in McNicol et al. (2021).

623 **UAV-LS data processing**

624 Flight trajectories were reconstructed using GNSS/IMU measurements and adjusted with differentially corrected base station
625 data in Applanix POSPac software. The corrected flight paths and laser data were then integrated using the RIEGL software
626 package, RiPROCESS, to generate the initial three-dimensional point cloud. Residual trajectory errors—such as discrepancies
627 in GPS tracking and elevation—were corrected by using small buildings as reference points to refine the relative position and
628 orientation of individual flight lines and scans. Further adjustments were made using ground control points: square targets (1–
629 2 m²) composed of alternating black and white material arranged in a checkerboard pattern. This process resulted in a LiDAR-
630 derived point cloud with a geometric accuracy of 1.8 cm. All elevation data were calculated as ellipsoidal heights (m) within
631 the UTM 32S coordinate system. Each flight was processed separately, and all datasets were merged prior to export.
632 Subsequent point cloud processing was carried out using elements of the lidR package (v3.1.0; Roussel et al., 2020). This
633 UAV-LS dataset is freely available via the Centre for Environmental Data Analysis (CEDA) with DOIs provided in section 5.
634 Data acquisition characteristics can be found in Table 6.

635

636 **Table 9:** Comparison of ALS acquisition characteristics for two ForestScan sites: FBRMS-01:Paracou, French Guiana and
637 FBRMS-03: Kabili-Sepilok, Malaysian Borneo. These key flight and sensor characteristics can support alignment and
638 comparability across sites.

ALS flight characteristics	FBRMS-01: Paracou, French Guiana	FBRMS-02: Kabili-Sepilok, Malaysian Borneo
Date	Nov 2019	Feb 2020
Area covered	10 km ²	27 km ² (Kabili-Sepilok) + 20 km ² (Danum Valley protected area) + 9 km ² (reduced impact logging area adjacent to Danum Valley)
Scanner	RIEGL LMS - Q780	RIEGL LMS - Q560
Platform	BN2 aircraft	Helicopter
Altitude	~900 m	~350 m (above forest canopy)
Speed	~180 km/h (50 m·s ⁻¹)	~100 km/h (30 m·s ⁻¹)
Scan angle	±30°	±30°
Pulse density	Min 15 pts/m ² ; Mean 40 pts/m ²	Mean 40 pts/m ²
Overlap	80%	40%
CRS	EPSG:2972	EPSG: 32650

639

640 **2.2.4 Airborne Laser Scanning (ALS)**

641 **FBRMS-01: Paracou, French Guiana**

642 ALS data were acquired over Paracou in November 2019. The data covers 10 km², including all experimental plots and areas
643 covered by TLS and UAV-LS (see Fig. 1). During the same campaign, additional data was gathered over Nouragues Research
644 Station in French Guiana. This supplementary data was collected using identical scanning characteristics (provided in Table
645 9) and has been incorporated into the ForestScan data archive.

646

647 ALS data for Paracou are freely available via the Centre for Environmental Data Analysis (CEDA) with DOIs provided in
648 section 5. Canopy height models for both Paracou and Sepilok are described in Jackson *et al.* (2024) and available at
649 <https://doi.org/10.908679>.

650 **FBRMS-03: Kabili-Sepilok, Malaysia**

651 ALS data were acquired at Kabili-Sepilok in February 2020. This dataset includes LiDAR and RedGreenBlue (RGB) imagery
652 data collected from a helicopter over the Kabili-Sepilok Forest Reserve and an additional non-ForestScan site -Danum Valley
653 Forest Reserve. These areas were selected due to the availability of prior ALS data collected in 2013 and 2014. The complete
654 collection and processing details for these datasets are detailed in Jackson *et al.* (2024).

655

656 The point cloud data for this FBRMS are available in LAS (LASer) format, as well as RGB data summary rasters in .tif format.
657 The raster images were processed with LAStools using default parameters. Canopy Height Model (CHM), Digital Surface
658 Model (DSM), Digital Terrain Model (DTM), and pulse density (pd) data are also included. The RGB data are provided in
659 .jpg format and organised by flight date. The data was georeferenced using ground control points. This ALS dataset is freely
660 available via the Centre for Environmental Data Analysis (CEDA) with DOIs provided in section 5.

661 **3. Recommendations for aligning and matching datasets**

662 We provide data that are internally consistent in terms of pre-processing, geo-referencing, and exported in formats compatible
663 with open-source tools. Any further processing will depend largely on the intended application, such as individual tree analysis
664 or plot-level studies.

665

666 For TLS data, all point clouds within a single plot are co-registered into one unified point cloud. These are subsequently
667 processed into individual tree point clouds, to which quantitative structural models (QSMs) are fitted to estimate volume.
668 Datasets for FBRMS-01 and FBRMS-02 were acquired using a RIEGL VZ-400i equipped with GNSS RTK positioning.

669 However, as GNSS performance is often compromised beneath dense tropical canopies, positional accuracy for these datasets
670 should be interpreted with caution.

671
672 UAV-LS and ALS datasets are geo-referenced in each case. As positional accuracy depends on the IMU and GNSS
673 measurements, which can introduce errors manifesting as height biases between individual flightlines. Although we did not
674 observe such discrepancies in our data, a rigorous comparison with ground control points would be required to confirm this
675 definitively -a step we have not undertaken. These datasets have not been explicitly aligned or matched to one another.
676 Alignment can be performed, but it requires manual identification of control points in each dataset and, as noted above, will
677 depend on the intended use of the resulting data.

678 **3.1 Matching TLS to census data: stem maps**

679 A key step in estimating AGB from tree-level terrestrial laser scanning (TLS) point clouds is the selection of wood density for
680 converting volume to mass. Wood density represents a significant source of uncertainty in the indirect estimation of AGB,
681 whether through allometry and census DBH, EO-derived canopy height, TLS-estimated volume, or other methods (Phillips et
682 al., 2019). If the censused trees in each plot can be matched to their TLS counterparts, literature estimates of species-specific
683 WD (or field-measured values, if available) can be used. In the absence of such a match, plot-level mean WD values are
684 employed, as is common in most EO-derived estimates that rely on large-scale allometric models (e.g. Chave et al., 2014).
685 Research by Momo et al. (2020), Burt et al. (2020), and Demol et al. (2021) has demonstrated that significant bias can occur
686 in TLS-derived AGB estimates due to within-tree WD variations when literature-derived species average WD values are used.
687 However, Momo et al. (2020) suggest there is sufficient correlation between vertical gradients and basal WD to allow for
688 empirical corrections.

689
690 While it is preferable to match TLS trees to census trees, this process is not straightforward and is currently only possible
691 manually (if at all) after TLS data acquisition and co-registration. Once registered, a slice through the TLS plot-level point
692 cloud can be generated, enabling the identification of individual trees from their stem profiles. This stem map can be provided
693 in hard copy or digital format (e.g., high-resolution PDF) to the census team, who can then revisit the plot, moving through it
694 in the same manner as during the census—starting at the plot’s southeast corner or 0,0 and moving up and down by 10 m
695 quadrants—annotating the TLS stem map with each tree census ID. This process can be conducted separately or as part of an
696 existing census but is best performed simultaneously or as soon as possible after TLS collection to minimise changes and
697 facilitate collaboration between TLS and census teams. Despite success with this approach in some plots (e.g., Gabon 2016),
698 experience has shown that significant understory, terrain variation, and/or changes and tree falls between census and TLS data
699 collection (e.g., ~2 years between census and TLS data collection for FBRMS-03 plots, and significant tree falls and changes
700 due to a storm between census and TLS data collection in FBRMS plot LPG-01 in Gabon) make this process very challenging,
701 particularly for smaller stems (in the 10-20 cm DBH range).

702 **3.2 Aligning TLS to UAV-LS data (and other spatial data)**

703 Through its accurate global registration via PPK processing, UAV-LS can be regarded as a high-quality geometric reference
704 for registration. For the purpose of comparison with accurate ALS data or satellite observations, a registration of TLS to the
705 UAV-LS point cloud is highly recommended. The integration of GNSS directly into TLS data collection now ensures that
706 registered plot-level point clouds are aligned within a global coordinate system. This significantly facilitates the co-registration
707 of TLS and UAV-LS point clouds, given that GNSS accuracy is typically within 1 metre. Historically, placing all LiDAR point
708 clouds within accurate global coordinate systems necessitated dedicated survey measurements of plot corners or TLS locations
709 via GNSS, a process often hindered by signal attenuation in dense forests. Consequently, GNSS surveying of plot corner
710 locations is not a standard component of forest census protocols, although it should be considered essential for plots intended
711 for EO calibration and validation purposes. The reduced cost of RTK GNSS equipment and its subsequent routine integration
712 into TLS workflows have made this more feasible, despite the challenges in obtaining fixed positions, and maintaining radio
713 link with a base positioned on a well-known point under deep forest canopy cover. While this may not benefit ALS directly,
714 UAV-LS is likely to serve as a valuable intermediary between TLS (and census data) and ALS. The requirement for global
715 GNSS positioning also extends to other spatial datasets.

716 **3.3 Aligning TLS and UAV-LS to ALS data**

717 Aligning ALS data with TLS and UAV-LS datasets presents significant challenges. Despite the use of high-quality GNSS
718 positioning, meter-scale geolocation discrepancies between sensors can occur. Co-locating LiDAR datasets acquired at
719 different scales -TLS, UAV-LS, and ALS- remains complex, with no standard or “turn-key” solution currently available.
720 Manual intervention is often required, and the approach varies by site and sensor combination. While plot-level AGB
721 estimation is relatively tolerant to these discrepancies, finer-scale applications (e.g., matching to tree-level census data) demand
722 more precise alignment. This can be partially addressed through manual co-registration using common tie points across
723 datasets.

724

725 Achieving meaningful alignment also depends on the internal characteristics of ALS point clouds. Acquisition parameters such
726 as point density, scan angle distribution, and footprint size influence comparability and should be controlled as far as possible.
727 Post-processing can regularise point density and scan angles within or across campaigns, improving consistency.
728 Homogeneous scanning geometry enables more stable structural metrics and enhances AGB prediction performance.
729 Similarly, parameters such as transmitted pulse power (which co-varies with pulse repetition rate) and flight altitude (affecting
730 footprint size and canopy penetration) should be standardised across acquisitions to minimise bias (Vincent et al., 2023). These
731 steps are critical for reducing alignment errors and ensuring robust comparisons between TLS, UAV-LS, and ALS datasets.

732 **4. Recommendations for data collection in FBRMS**

733 Building on this first case study, we make the following general recommendations for data collection of tropical forest plot
734 census, TLS, UAV-LS and ALS data for the specific application of estimating AGB and upscaling to EO estimates. These
735 recommendations follow from the CEOS LPV AGB protocol and subsequent requirements identified for the GEO-TREES
736 initiative.

737 • **Consistent data acquisition and processing:** in order to facilitate the comparison of AGB estimates between sites,
738 dates, teams, etc. care should be taken to collect and process data as consistently as possible. This might seem obvious
739 but is particularly important as the use of TLS and UAV-LS for AGB estimation (and even ALS in some cases) are
740 currently primarily research-led (as opposed to fully operational). As new methods and tools are developed, including
741 newer versions of existing software, care should be taken to ensure backwards compatibility of the resulting AGB
742 estimates. This means either re-processing older data, or at the very least, some form of cross-comparison of original
743 and new methods. In our experience, listed below are some of the areas where care is needed to ensure data
744 consistency and reduce bias and uncertainty:

745 • **TLS data acquisition** - comparison between sites and plots is made much easier by using the same census,
746 TLS, UAV-LS and ALS data acquisition and processing protocols. Even within the forest plot census
747 community there are slightly different protocols and processes between different plot networks. This is even
748 more variable for different sources of LiDAR data. We note that much of the TLS work in tropical forests
749 aimed at volume reconstruction and AGB estimation has been carried out with RIEGL VZ series TLS
750 instruments. We make no comment as to what is ‘the best’ instrument - there are various cost/benefit trade-
751 offs to be made. Equipment has to be robust to withstand tropical forest work (and humidity). LiDAR range
752 needs to be in the 100s of metres to ensure points are returned from tall canopies. Phase-shift TLS systems
753 can be light and have very rapid scan rates, but suffer from ‘ghosting’ of multiple returned hits along a beam
754 path. Mobile Laser Scanning (MLS) systems offer rapid coverage, and require minimal input for registration
755 by using simultaneous location and mapping (SLAM), but tend to have lower range and precision due to the
756 uncertainty in absolute location resulting from SLAM. It is likely that these systems will become more
757 powerful and precise, offering a possible alternative to static tripod-mounted TLS in the future for AGB
758 applications. Specific issues to consider are TLS power. For example, the RIEGL VZ-400 and newer VZ-
759 400i systems (both used here) have different recording sensitivities i.e. down to -30 dB for the newer VZ-
760 400i, whereas the VZ-400 only recorded to -20 dB. This can have a significant impact on the number of
761 returns, particularly from further away and higher in the canopy and should be taken into consideration when
762 comparing results between older and newer TLS instruments. Choices are also possible in terms of power
763 settings: lower power settings reduce scan times & extend battery time, but also significantly reduce the
764 quality of resulting point clouds, particularly higher in the canopy. TLS data were collected using a pulse
765 repetition rate (PRR) of 300 kHz on RIEGL VZ-400 and VZ-400i scanners, trading longer scan times for a

766 fixed angular resolution to maximise coverage at the tops of tall trees. In the RIEGL configuration, PRR and
767 emitted laser power are intrinsically linked: increasing the PRR reduces the available power, and vice versa.
768 Consequently, the choice of PRR determines the power setting, and adjustments to one parameter necessarily
769 influence the other. However, recent work by Verhertz et al. (2024) suggests that using lower power, but
770 with higher angular resolution, can achieve better coverage in tall forests for the same scan duration (3 mins
771 per scan). More generally, comparing measurements made with scanners of varying power, sensitivity,
772 resolution etc. will compound uncertainties (particularly biases) in the resulting estimates of AGB and so
773 should be avoided or minimised as far as possible. This is particularly important for large-scale site-to-site
774 comparison required for EO biomass product cal/val (e.g. for global FBRMS comparisons).

775

- 776 **TLS processing** - broadly, TLS data acquisition and processing in tropical forests has gradually converged
777 towards something of a consensus, albeit this is still an active area of research and will vary depending on
778 the team, site and application. Specific issues to consider are the way in which trees are extracted from plot-
779 scale point clouds. Currently, the most accurate method for doing this is by manual cleaning of each tree
780 using a tool such as CloudCompare (CloudCompare Development Team, 2025). However, this is a time-
781 consuming and somewhat subjective process that is not fully replicable - different people will produce
782 slightly different results. Automated pipelines using machine learning/deep learning (ML/DL) offer a more
783 rapid and repeatable approach (e.g. Krisanski et al., 2021; Wilkes et al., 2023), however, their resulting tree
784 extraction accuracy is harder to assess given that the 'true' structure of trees is unknown. Manually-extracted
785 trees can be used to assess automated tree extraction accuracy, as well as forming the training data to enable
786 improvements in the underlying ML/DL approaches. Developing locally-trained / optimised ML/DL models
787 is likely to improve this approach further. Moving from individual tree point clouds to volume estimates it
788 is also important to use consistent QSM-fitting approaches. For example, there are systematic differences
789 between older and newer versions of TreeQSM, currently the most widely-used QSM fitting software
790 (Demol et al., 2024; Raumonen et al., 2013). Quantifying the uncertainty in tree-level estimates of volume
791 will depend on this processing chain, which will then determine the plot-level uncertainty when upscaling.
- 792 **UAV-LS acquisition and processing** - due to the wide range of platforms and LiDAR payloads being used
793 (as well as local UAV and safety regulations), there is currently little consensus in terms of both acquisition
794 and processing of UAV-LS data. There are a wide range of flight choices (particularly altitude), instrument
795 settings (scan angle), and survey systems (overlap, duration, etc.) that are a function of platform
796 performance, cost, etc. The impact of some of these choices is discussed in Brede et al. (2022b) where the
797 benefits of higher power, multiple returns and overlapping flights in detecting canopy structure are
798 highlighted. UAV-LS is not a like-for-like replacement for TLS, thus, the ability to compare these two
799 different sources of LiDAR data will be facilitated by accurate geo-location (see above). This can be
achieved by using ground targets with surveyed locations that can be identified in the UAV-LS data (e.g.

reflective sheets/tarps, umbrellas, commercial UAV targets etc). This presupposes that there are sufficient gaps in the canopy for targets to be seen, which is not always true. During data collection attention should be paid to also either have access to GNSS observables from permanent base stations (e.g. CORS network) or collect observables with a temporary base station (e.g. Emlid Reach RS+ or RS2). A base station should be positioned less than 15 km away from the survey area. An important consideration for UAV-LS data collection is whether visual line of sight VLOS needs to be maintained, i.e. visibility of the platform by the pilot during the whole mission. If so, this can impact the choice of take-off, flight plan, etc. which in turn may influence the choice of platform. Fixed-wing platforms have a much greater area coverage and flight duration than VTOL platforms, but by necessity, must operate beyond VLOS (BVLOS). They also require far more space to take off and land than VTOL platforms.

- **ALS acquisition and processing** - while ALS has been used operationally for forest applications for several decades, its application for AGB estimates specifically is still less well-defined. In particular, this is true when considering tree-scale rather than plot-level estimates. Practically, ALS surveys are almost always outsourced (from the plot PIs, census and TLS, UAV teams) to commercial or agency (e.g. NASA, ESA, NERC) providers. In the former case, there may be limited input from the end user over the platform, instrument and acquisition parameters, or the way in which the data are processed to the resulting final delivery. In ESA, NERC, NASA acquisitions, there tends to be more input from the users, but there may be other restrictions in terms of when and where flights can be made. We recommend a pulse density of 10 m^{-2} or higher and a swath angle of +/-15 degrees or smaller. Most importantly, consistency over time of the other acquisition parameters should be sought to enable meaningful temporal analysis of ALS point cloud. In most cases, the 3D point cloud will be processed to generate a 2D canopy height model for further analysis. This post-processing can have important effects on the results, we therefore, recommend users follow a standardized procedure such as Fischer et al. (2024).
- **Accurate (cm-scale) GNSS locations for 1ha FBRMS plot corners (or at the least the nominal origin 0, 0 coordinate for each plot):** this makes comparison and merging of any subsequent measurements much easier. It is important to note that this is not a standard requirement of forest census measurements and requires specialist surveying equipment e.g. GNSS RTK base station + rover configuration. It is also challenging under heavy forest cover. Given that such setups are required (ideally) for TLS and UAV-LS, plot corner surveying is potentially best carried out by these teams.
- **Linking TLS trees to their census counterparts:** ideally, a permanent $10 \times 10\text{m}$ subplot grid would be established within each 1 ha forest plot. Census teams can then follow the same chain sampling pattern used in TLS data collection (see Figure 2.1.4b & c) and identify the tree IDs found within each $10 \times 10 \text{ m}$ quadrants as they move through the plot. However, placing a $10 \times 10 \text{ m}$ sub-grid is not always straightforward (or even desirable) as it may require rebar posts, which can be expensive and are likely to be removed or damaged by e.g. elephants in West African plots

834 particularly. An alternative approach is to label some trees with temporary numbered QR-type markers that can be
835 read automatically from the lidar point cloud data. The markers can be printed on A4 waterproof paper, attached to
836 trees with known census ID, and then identified in the TLS data using a tool such as qrDAR (Wilkes et al., 2017). If
837 the 20 or so largest trees are labelled in this way, distributed across a 1 ha plot, this makes subsequent tree matching
838 between census and TLS data much easier as there are known ‘anchor trees’ for the survey team to work from.

839 **5. Data Access**

840 This paper presents 30 datasets, comprising LiDAR and tree census data for all three ForestScan FBRMS. All datasets are
841 archived and publicly accessible through established data repositories. LiDAR datasets, including TLS, UAV-LS and ALS are
842 freely available from the CEDA Archive (<https://archive.ceda.ac.uk>) under the ForestScan data collection
843 (<https://dx.doi.org/10.5285/88a8620229014e0ebacf0606b302112d>; Chavana-Bryant et al., 2025b). This collection serves as
844 an umbrella repository linking all individual LiDAR datasets by site and acquisition type. All tree census datasets are provided
845 as curated data packages made available by the ForestPlots consortium and the French Agricultural Research Centre for
846 International Development (CIRAD) open-access portal.

847
848 Tree census data packages for all three FBRMS are made available via two archival platforms: the CIRAD DataVerse portal
849 for French Guiana (<https://dataVERSE.cirad.fr/dataset.xhtml?persistentId=doi:10.18167/DVN1/94XHID>; Derroire et al., 2025),
850 while Gabon and Malaysian Borneo data are available through ForestPlots.net (https://doi.org/10.5521/forestplots.net/2025_2;
851 Chavana-Bryant et al., 2025a). An additional census dataset for a non-ForestScan plot at FBRMS-01 is included in Table 10
852 and made available via the CEDA archive.

853
854 Both tree census archival platforms operate under a fair use policy, governed by the Creative Commons Attribution-
855 NonCommercial-ShareAlike 4.0 International Licence (CC BY-NC-SA 4.0) (see <https://forestplots.net/en/join-forestplots/working-with-data> and <https://dataVERSE.org/best-practices/dataVERSE-community-norms>). These policies reflect a
856 strong commitment to equitable and inclusive data collection, funding, and sharing practices, as outlined in the ForestPlots
857 code of conduct (<https://forestplots.net/en/join-forestplots/code-of-conduct>). Tropical forest plot census data provide unique
858 insights into forest structure and dynamics but are challenging and often hazardous to collect, requiring sustained investment
859 and logistical support in remote regions with limited infrastructure. A persistent challenge to equitable research is that those
860 who collect these data are often least able to exploit the resulting large-scale datasets. This issue is particularly acute in the
861 context of commercial data exploitation, including by artificial intelligence and large-scale data mining enterprises. To address
862 this, the ForestPlots community has developed data-sharing agreements that promote fairness and inclusivity, as detailed in de
863 Lima et al. (2022).

866 Access and citation details for all ForestScan datasets are organised by site in Tables 10, 11, and 12 for FBRMS-01: Paracou,
867 French Guiana, FBRMS-02: Lopé National Park, Gabon, and FBRMS-03: Sepilok-Kabili, Malaysian Borneo, respectively.
868 Each table provides the specific data type, acquisition date, license type and citation format including DOI and URL for each
869 individual ForestScan dataset.

870

871 **Table 10:** Dataset type, acquisition date, license type, and citation format including DOI and URL details for LiDAR (TLS,
872 UAV-LS and ALS) and tree census datasets available for FBRMS-01: Paracou, French Guiana. When using any of the
873 ForestScan datasets, this paper must also be cited.

ForestScan French Guiana Datasets / Acquisition date / Data license type	Data type	Citable as (DOI and URL included)
ForestScan Collection	Collection (multi-type composite of all ForestScan CEDA datasets)	Chavana-Bryant, C.; Wilkes, P.; Yang, W.; Burt, A.; Vines, P.; Bennett, A.C.; Pickavance, G.C.; Cooper, D.L.M.; Lewis, S.L.; Phillips, O.L.; Brede, B.; Lau, A.; Herold, M.; McNicol, I.M.; Mitchard, E.T.A.; Coombes, D.; Jackson, T.D.; Makaga, L.; Milamizokou Napo, H.O.; Ngomanda, A.; Ntie, S.; Medjibe, V.; Dimbonda, P.; Soenens, L.; Daelemans, V.; Proux, L.; Nilus, R.; Labrière, N.; Jeffery, K.; Burslem, D.F.R.P.; Clewley, D.; Moffat, D.; Qie, L.; Bartholomeus, H.; Vincent, G.; Barbier, N.; Derroire, G.; Abernethy, K.; Scipal, K.; Disney, M. (2025): ForestScan Collection. NERC EDS Centre for Environmental Data Analysis, 20 January 2025. DOI:10.5285/88a8620229014e0ebacf0606b302112d. https://catalogue.ceda.ac.uk/uuid/88a8620229014e0ebacf0606b302112d
ForestScan Project: Terrestrial Laser Scanning (TLS) of FBRMS-01: Paracou, French Guiana 1ha plot FG5c1 Acquisition date: Sep - Oct 2022 License type: CC BY 4.0 http://creativecommons.org/licenses/by/4.0/	TLS	Chavana-Bryant, C.; Wilkes, P.; Yang, W.; Burt, A.; Vines, P.; Bennett, A.C.; Pickavance, G.C.; Cooper, D.L.M.; Lewis, S.L.; Phillips, O.L.; Brede, B.; Lau, A.; Herold, M.; McNicol, I.M.; Mitchard, E.T.A.; Coombes, D.; Jackson, T.D.; Makaga, L.; Milamizokou Napo, H.O.; Ngomanda, A.; Ntie, S.; Medjibe, V.; Dimbonda, P.; Soenens, L.; Daelemans, V.; Proux, L.; Nilus, R.; Labrière, N.; Jeffery, K.; Burslem, D.F.R.P.; Clewley, D.; Moffat, D.; Qie, L.; Bartholomeus, H.; Vincent, G.; Barbier, N.; Derroire, G.; Abernethy, K.; Scipal, K.; Disney, M. (2025): ForestScan Project : Terrestrial Laser Scanning (TLS) of FBRMS-01: Paracou, French Guiana 1ha plot FG5c1, September to October 2022. NERC EDS Centre for Environmental Data Analysis, 28 March 2025. DOI:10.5285/656ac8ee1d42443f9addcbce28c1b137.

		https://dx.doi.org/10.5285/656ac8ee1d42443f9addcbce28c1b137
ForestScan Project: Terrestrial Laser Scanning (TLS) of FBRMS-01: Paracou, French Guiana 1ha plot FG6c2 Acquisition date: Sep - Oct 2022 License type: CC BY 4.0 http://creativecommons.org/licenses/by/4.0/	TLS	Chavana-Bryant, C.; Wilkes, P.; Yang, W.; Burt, A.; Vines, P.; Bennett, A.C.; Pickavance, G.C.; Cooper, D.L.M.; Lewis, S.L.; Phillips, O.L.; Brede, B.; Lau, A.; Herold, M.; McNicol, I.M.; Mitchard, E.T.A.; Coombes, D.; Jackson, T.D.; Makaga, L.; Milamizokou Napo, H.O.; Ngomanda, A.; Ntie, S.; Medjibe, V.; Dimbonda, P.; Soenens, L.; Daelemans, V.; Proux, L.; Nilus, R.; Labrière, N.; Jeffery, K.; Burslem, D.F.R.P.; Clewley, D.; Moffat, D.; Qie, L.; Bartholomeus, H.; Vincent, G.; Barbier, N.; Derroire, G.; Abernethy, K.; Scipal, K.; Disney, M. (2025): ForestScan Project : Terrestrial Laser Scanning (TLS) of FBRMS-01: Paracou, French Guiana 1ha plot FG6c2, September to October 2022. NERC EDS Centre for Environmental Data Analysis, 28 March 2025. DOI:10.5285/931973db09af41568853702efe135f29. https://dx.doi.org/10.5285/931973db09af41568853702efe135f29
ForestScan Project: Terrestrial Laser Scanning (TLS) of FBRMS-01: Paracou, French Guiana 1ha plot FG8c4 Acquisition date: Sep - Oct 2022 License type: CC BY 4.0 http://creativecommons.org/licenses/by/4.0/	TLS	Chavana-Bryant, C.; Wilkes, P.; Yang, W.; Burt, A.; Vines, P.; Bennett, A.C.; Pickavance, G.C.; Cooper, D.L.M.; Lewis, S.L.; Phillips, O.L.; Brede, B.; Lau, A.; Herold, M.; McNicol, I.M.; Mitchard, E.T.A.; Coombes, D.; Jackson, T.D.; Makaga, L.; Milamizokou Napo, H.O.; Ngomanda, A.; Ntie, S.; Medjibe, V.; Dimbonda, P.; Soenens, L.; Daelemans, V.; Proux, L.; Nilus, R.; Labrière, N.; Jeffery, K.; Burslem, D.F.R.P.; Clewley, D.; Moffat, D.; Qie, L.; Bartholomeus, H.; Vincent, G.; Barbier, N.; Derroire, G.; Abernethy, K.; Scipal, K.; Disney, M. (2025): ForestScan Project : Terrestrial Laser Scanning (TLS) of FBRMS-01: Paracou, French Guiana 1ha plot FG8c4, September to October 2022. NERC EDS Centre for Environmental Data Analysis, 28 March 2025. DOI:10.5285/40f0f38023ac40f6b40bbf96e4dc5258. https://dx.doi.org/10.5285/40f0f38023ac40f6b40bbf96e4dc5258
ForestScan: Terrestrial Laser Scanning (TLS) of FBRMS-01: Paracou, French Guiana 1ha plot IRD-CNES (Tropiscat) Acquisition date: Oct 2021 License type: CC BY 4.0	TLS	Vincent, G.; Villard, L. (2025): ForestScan: Terrestrial Laser Scanning (TLS) of FBRMS-01: Paracou, French Guiana 1ha plot IRD-CNES, October 2021. NERC EDS Centre for Environmental Data Analysis, 28 March 2025. DOI:10.5285/b1cd34f6af7941a3b1429ac52a3f6b28. h

http://creativecommons.org/licenses/by/4.0/		https://dx.doi.org/10.5285/b1cd34f6af7941a3b1429ac52a3f6b28
ForestScan Project: Unpiloted Aerial Vehicle LiDAR Scanning (UAV-LS) and Terrestrial Laser Scanning (TLS) data of FBRMS-01: Paracou, French Guiana plot 6 Acquisition date: Oct – Nov 2019 License type: CC BY 4.0 http://creativecommons.org/licenses/by/4.0/	UAV-LS + TLS	Brede, B.; Barbier, N.; Bartholomeus, H.; Derroire, G.; Lau, A.; Lusk, D.; Herold, M. (2025): ForestScan Project: Unpiloted Aerial Vehicle LiDAR Scanning (UAV-LS) and Terrestrial Laser Scanning (TLS) data of FBRMS-01: Paracou, French Guiana plot 6, 10th October to 15th November 2019. NERC EDS Centre for Environmental Data Analysis, <i>28 March 2025</i> . DOI:10.5285/325a4dde60d142049339e0c84816aac1. https://dx.doi.org/10.5285/325a4dde60d142049339e0c84816aac1
ForestScan Project: Multiple Unpiloted Aerial Vehicle LiDAR Scanning (UAV-LS) data acquisitions of FBRMS-01: Paracou, French Guiana, plots 4, 5, 6, 8, IRD-CNRS (Tropiscat) and Flux-Tower area Acquisition date: Oct 2019 License type: CC BY 4.0 http://creativecommons.org/licenses/by/4.0/	UAV-LS	Barbier, N.; Vincent, G. (2025): ForestScan Project: Multiple Unpiloted Aerial Vehicle LiDAR Scanning (UAV-LS) data acquisitions of FBRMS-01: Paracou, French Guiana, plots 4, 5, 6, 8, IRD-CNRS and Flux-Tower area, October 2019. NERC EDS Centre for Environmental Data Analysis, <i>28 March 2025</i> . DOI:10.5285/005f2e0aebc24ed98a9772a0ba3798e2. https://dx.doi.org/10.5285/005f2e0aebc24ed98a9772a0ba3798e2
ForestScan: Aerial Laser Scanning (ALS) of FBRMS-01: Paracou, French Guiana Acquisition date: Nov 2022 License type: CC BY 4.0 http://creativecommons.org/licenses/by/4.0/	ALS	Vincent, G. (2025): ForestScan: Aerial Laser Scanning (ALS) of FBRMS-01: Paracou, French Guiana, November 2022. NERC EDS Centre for Environmental Data Analysis, <i>28 March 2025</i> . DOI:10.5285/7bef89a9dc404683a46642625a024a4b. https://dx.doi.org/10.5285/7bef89a9dc404683a46642625a024a4b
Aerial LiDAR (ALS) French Guiana Paracou Acquisition date: Nov 2019 License type: CC BY 4.0 http://creativecommons.org/licenses/by/4.0/	ALS	Jackson, T.D.; Vincent, G.; Coomes, D.A. (2023): Aerial LiDAR data from French Guiana, Paracou, November 2019. NERC EDS Centre for Environmental Data Analysis, <i>20 December 2023</i> . DOI:10.5285/1d554ff41c104491ac3661c6f6f52aab. https://dx.doi.org/10.5285/1d554ff41c104491ac3661c6f6f52aab
Aerial LiDAR (ALS) French Guiana Nouragues Acquisition date: Nov 2019 License type: CC BY 4.0 http://creativecommons.org/licenses/by/4.0/	ALS (additional non-ForestScan plot)	Jackson, T.D.; Vincent, G.; Coomes, D.A. (2023): Aerial LiDAR data from French Guiana, Nouragues, November 2019. NERC EDS Centre for Environmental Data Analysis, <i>20 December 2023</i> . DOI:10.5285/7bdc5bfc06264802be34f918597150e8. https://dx.doi.org/10.5285/7bdc5bfc06264802be34f918597150e8

<p>ForestScan: Plot descriptions for FBRMS-01: Paracou, French Guiana, 1ha plots FG5c1, FG6c2 and FG8c4</p> <p>License: CC BY-NC-SA 4.0</p> <p>http://creativecommons.org/licenses/by-nc-sa/4.0/</p>	<p>Tree census plot descriptions</p>	<p>Derroire, G., Hérault, B., Rossi, V., Blanc, L., Gourlet-Fleury, S., Schmitt, L., 2025, "ForestScan", 10.18167/DVN1/94XHID, CIRAD Dataverse, V1</p> <p>https://dataVERSE.cirad.fr/dataset.xhtml?persistentId=doi:10.18167/DVN1/94XHID</p>
<p>ForestScan: Tree census data for FBRMS-01: Paracou, French Guiana, 1ha plots FG5c1, FG6c2 and FG8c4</p> <p>Acquisition date: FG5c1: Aug 2023 FG6c2: May - Jun 2023 FG8c4: Sep 2023</p> <p>License: CC BY-NC-SA 4.0</p> <p>http://creativecommons.org/licenses/by-nc-sa/4.0/</p>	<p>Tree census</p>	<p>Derroire, G., Hérault, B., Rossi, V., Blanc, L., Gourlet-Fleury, S., Schmitt, L., 2025, "ForestScan", 10.18167/DVN1/94XHID, CIRAD Dataverse, V1</p> <p>https://dataVERSE.cirad.fr/dataset.xhtml?persistentId=doi:10.18167/DVN1/94XHID</p>
<p>ForestScan: Tree census data (diameter and species name) of FBRMS-01: Paracou, French Guiana 1ha plot IRD-CNES (Tropiscat)</p> <p>Acquisition date: Oct 2021</p> <p>License type: CC BY 4.0</p> <p>http://creativecommons.org/licenses/by/4.0/</p>	<p>Tree census (additional non-ForestScan plot)</p>	<p>Vincent, G.; Martin, O.; Engel, F. (2025): ForestScan: Tree census data (diameter and species name) of FBRMS-01: Paracou, French Guiana 1ha plot IRD-CNES, October 2021. NERC EDS Centre for Environmental Data Analysis, 28 March 2025. DOI:10.5285/5e78ff91e9cd4143bfa3b7358efd2607. https://dx.doi.org/10.5285/5e78ff91e9cd4143bfa3b7358efd2607</p>

874

875 **Table 10:** Dataset type, acquisition date, license type, and citation format including DOI and URL details for LiDAR (TLS,
 876 UAV-LS and ALS) and tree census datasets available for FBRMS-02: Lopé, Gabon. When using any of the ForestScan
 877 datasets, this paper must also be cited.

ForestScan Gabon Datasets / Acquisition date / Data license type	Data type	Citable as (DOI and URL included)
<p>ForestScan Project : Terrestrial Laser Scanning (TLS) of FBRMS-02: Station d'Etudes des Gorilles et Chimpanzés, Lopé National Park, Gabon 1ha plot LPG-01</p> <p>Acquisition date: Jun - Jul 2022</p> <p>License type: CC BY 4.0</p> <p>http://creativecommons.org/licenses/by/4.0/</p>	<p>TLS</p>	<p>Chavana-Bryant, C.; Wilkes, P.; Yang, W.; Burt, A.; Vines, P.; Bennett, A.C.; Pickavance, G.C.; Cooper, D.L.M.; Lewis, S.L.; Phillips, O.L.; Brede, B.; Lau, A.; Herold, M.; McNicol, I.M.; Mitchard, E.T.A.; Coombes, D.; Jackson, T.D.; Makaga, L.; Milamizokou Napo, H.O.; Ngomanda, A.; Ntie, S.; Medjibe, V.; Dimbona, P.; Soenens, L.; Daelemans, V.; Proux, L.; Nilus, R.; Labrière, N.; Jeffery, K.; Burslem, D.F.R.P.; Clewley, D.; Moffat, D.; Qie, L.;</p>

		Bartholomeus, H.; Vincent, G.; Barbier, N.; Derroire, G.; Abernethy, K.; Scipal, K.; Disney, M. (2025): ForestScan Project : Terrestrial Laser Scanning (TLS) of FBRMS-02: Station d'Etudes des Gorilles et Chimpanzés, Lopé National Park, Gabon 1ha plot LPG-01, June to July 2022. NERC EDS Centre for Environmental Data Analysis, 28 March 2025. DOI:10.5285/8ea2c697ee53430a84825384bfdcf06a. https://dx.doi.org/10.5285/8ea2c697ee53430a84825384bfdcf06a
ForestScan Project : Terrestrial Laser Scanning (TLS) of FBRMS-02: Station d'Etudes des Gorilles et Chimpanzés, Lopé National Park, Gabon 1ha plot OKO-01 Acquisition date: Jun - Jul 2022 License type: CC BY 4.0 http://creativecommons.org/licenses/by/4.0/	TLS	Chavana-Bryant, C.; Wilkes, P.; Yang, W.; Burt, A.; Vines, P.; Bennett, A.C.; Pickavance, G.C.; Cooper, D.L.M.; Lewis, S.L.; Phillips, O.L.; Brede, B.; Lau, A.; Herold, M.; McNicol, I.M.; Mitchard, E.T.A.; Coombes, D.; Jackson, T.D.; Makaga, L.; Milamizokou Napo, H.O.; Ngomanda, A.; Ntie, S.; Medjibe, V.; Dimbonda, P.; Soenens, L.; Daelemans, V.; Proux, L.; Nilus, R.; Labrière, N.; Jeffery, K.; Burslem, D.F.R.P.; Clewley, D.; Moffat, D.; Qie, L.; Bartholomeus, H.; Vincent, G.; Barbier, N.; Derroire, G.; Abernethy, K.; Scipal, K.; Disney, M. (2025): ForestScan Project : Terrestrial Laser Scanning (TLS) of FBRMS-02: Station d'Etudes des Gorilles et Chimpanzés, Lopé National Park, Gabon 1ha plot OKO-01, June to July 2022. NERC EDS Centre for Environmental Data Analysis, 28 March 2025. DOI:10.5285/45ae3437f82f4e4fb75f9a5c26a194ba. https://dx.doi.org/10.5285/45ae3437f82f4e4fb75f9a5c26a194ba
ForestScan Project : Terrestrial Laser Scanning (TLS) of FBRMS-02: Station d'Etudes des Gorilles et Chimpanzés, Lopé National Park, Gabon 1ha plot OKO-02 Acquisition date: Jun - Jul 2022 License type: CC BY 4.0 http://creativecommons.org/licenses/by/4.0/	TLS	Chavana-Bryant, C.; Wilkes, P.; Yang, W.; Burt, A.; Vines, P.; Bennett, A.C.; Pickavance, G.C.; Cooper, D.L.M.; Lewis, S.L.; Phillips, O.L.; Brede, B.; Lau, A.; Herold, M.; McNicol, I.M.; Mitchard, E.T.A.; Coombes, D.; Jackson, T.D.; Makaga, L.; Milamizokou Napo, H.O.; Ngomanda, A.; Ntie, S.; Medjibe, V.; Dimbonda, P.; Soenens, L.; Daelemans, V.; Proux, L.; Nilus, R.; Labrière, N.; Jeffery, K.; Burslem, D.F.R.P.; Clewley, D.; Moffat, D.; Qie, L.; Bartholomeus, H.; Vincent, G.; Barbier, N.; Derroire, G.; Abernethy, K.; Scipal, K.; Disney, M. (2025): ForestScan Project : Terrestrial Laser Scanning (TLS) of FBRMS-02: Station d'Etudes des Gorilles et Chimpanzés, Lopé National Park, Gabon 1ha plot OKO-02, June to July 2022. NERC EDS Centre for Environmental Data Analysis, 28 March 2025. DOI:10.5285/ff4b43475c9641cca1dad2c8be8dadaf. https://dx.doi.org/10.5285/ff4b43475c9641cca1dad2c8be8dadaf

<p>ForestScan Project : Terrestrial Laser Scanning (TLS) of FBRMS-02: Station d'Etudes des Gorilles et Chimpanzés, Lopé National Park, Gabon 1ha plot OKO-03</p> <p>Acquisition date: Jun - Jul 2022</p> <p>License type: CC BY 4.0 http://creativecommons.org/licenses/by/4.0/</p>	<p>TLS</p>	<p>Chavana-Bryant, C.; Wilkes, P.; Yang, W.; Burt, A.; Vines, P.; Bennett, A.C.; Pickavance, G.C.; Cooper, D.L.M.; Lewis, S.L.; Phillips, O.L.; Brede, B.; Lau, A.; Herold, M.; McNicol, I.M.; Mitchard, E.T.A.; Coombes, D.; Jackson, T.D.; Makaga, L.; Milamizokou Napo, H.O.; Ngomanda, A.; Ntie, S.; Medjibe, V.; Dimbonda, P.; Soenens, L.; Daelemans, V.; Proux, L.; Nilus, R.; Labrière, N.; Jeffery, K.; Burslem, D.F.R.P.; Clewley, D.; Moffat, D.; Qie, L.; Bartholomeus, H.; Vincent, G.; Barbier, N.; Derroire, G.; Abernethy, K.; Scipal, K.; Disney, M. (2025): ForestScan Project : Terrestrial Laser Scanning (TLS) of FBRMS-02: Station d'Etudes des Gorilles et Chimpanzés, Lopé National Park, Gabon 1ha plot OKO-03, June to July 2022. NERC EDS Centre for Environmental Data Analysis, 28 March 2025. DOI:10.5285/8ed3ddec76b8470285bdb2ea643f54bc. https://dx.doi.org/10.5285/8ed3ddec76b8470285bdb2ea643f54bc</p>
<p>ForestScan project: Unpiloted Aerial Vehicle LiDAR Scanning (UAV-LS) data of FBRMS-02: Station d'Etudes des Gorilles et Chimpanzés, Lopé National Park, Gabon</p> <p>Acquisition date: Jun 2022</p> <p>License type: CC BY 4.0 http://creativecommons.org/licenses/by/4.0/</p>	<p>UAV-LS</p>	<p>McNicol, I.M.; Mitchard, E.T.A. (2025): ForestScan project: Unpiloted Aerial Vehicle LiDAR Scanning (UAV-LS) data of FBRMS-02: Station d'Etudes des Gorilles et Chimpanzés, Lopé National Park, Gabon, June 2022. NERC EDS Centre for Environmental Data Analysis, 28 March 2025. DOI: 10.5285/a79fcb9ab0c443fc86d453cc064759b. https://dx.doi.org/10.5285/a79fcb9ab0c443fc86d453cc064759b1</p>
<p>ForestScan: Tree census data for FBRMS-02: Lope, Gabon, 1ha plots LPG-01, OKO-01, OKO-02 and OKO-03</p> <p>Acquisition date: LPG-01: Feb 2022 OKO-01: Mar 2022 OKO-02: Feb 2022 OKO-03: Feb 2022</p> <p>License: CC BY-NC-SA 4.0 http://creativecommons.org/licenses/by-nc-sa/4.0/</p>	<p>Tree census</p>	<p>Chavana-Bryant, C., Wilkes, P., Yang, W., Burt, A., Vines, P., Bennett, A.C., Pickavance, G., Cooper, D.L.M., Lewis, S.L., Phillips, O.L., Brede, B., Lau, A., Herold, M., McNicol, I.M., Mitchard, E.T.A., Barbier, N., Vincent, G., Coomes, D.A., Jackson, T., Makaga, L., Milamizokou Napo, H.O., Ngomanda, A., Ntie, S., Medjibe, V., Dimbonda, P., Soenens, L., Daelemans, V., Bartholomeus, H., Majalap, N., Nilus, R., Labrière, N., Burslem, D.F.R.P., Qie, L., Derroire, G., Proux, L., Abernethy, K., Jeffery, K., Clewley, D., Moffat, D., Scipal, K. and Disney, M. ForestScan: a unique multiscale dataset of tropical forest structure across 3 continents including terrestrial, UAV and airborne LiDAR and in-situ forest census data. ESSD. 2025 DOI: 10.5521/forestplots.net/2025_2 https://doi.org/10.5521/forestplots.net/2025_2</p>

879 **Table 11:** Dataset type, acquisition date, license type, and citation format including DOI and URL details for LiDAR (TLS,
 880 UAV-LS and ALS) and tree census datasets available for FBRMS-03: Kabili-Sepilok, Malaysian Borneo. When using any of
 881 the ForestScan datasets, this paper must also be cited.

ForestScan Malaysian Borneo Datasets / Acquisition date / Data license type	Data type	Citable as (DOI and URL included)
ForestScan Project : Terrestrial Laser Scanning (TLS) of FBRMS-03: Kabili-Sepilok, Malaysian Borneo 1ha plot SEP-11 Acquisition date: Mar 2017 License type: CC BY 4.0 http://creativecommons.org/licenses/by/4.0/	TLS	Chavana-Bryant, C.; Wilkes, P.; Yang, W.; Burt, A.; Vines, P.; Bennett, A.C.; Pickavance, G.C.; Cooper, D.L.M.; Lewis, S.L.; Phillips, O.L.; Brede, B.; Lau, A.; Herold, M.; McNicol, I.M.; Mitchard, E.T.A.; Coombes, D.; Jackson, T.D.; Makaga, L.; Milamizokou Napo, H.O.; Ngomanda, A.; Ntie, S.; Medjibe, V.; Dimbonda, P.; Soenens, L.; Daelemans, V.; Proux, L.; Nilus, R.; Labrière, N.; Jeffery, K.; Burslem, D.F.R.P.; Clewley, D.; Moffat, D.; Qie, L.; Bartholomeus, H.; Vincent, G.; Barbier, N.; Derroire, G.; Abernethy, K.; Scipal, K.; Disney, M. (2025): ForestScan Project : Terrestrial Laser Scanning (TLS) of FBRMS-03: Kabili-Sepilok, Malaysian Borneo 1ha plot SEP-11, March 2017. NERC EDS Centre for Environmental Data Analysis, 28 March 2025. DOI:10.5285/37b039605e9b4bb5a89371fd7f5b7ba1. https://dx.doi.org/10.5285/37b039605e9b4bb5a89371fd7f5b7ba1
ForestScan Project : Terrestrial Laser Scanning (TLS) of FBRMS-03: Kabili-Sepilok, Malaysian Borneo 1ha plot SEP-12 Acquisition date: Mar 2017 License type: CC BY 4.0 http://creativecommons.org/licenses/by/4.0/	TLS	Chavana-Bryant, C.; Wilkes, P.; Yang, W.; Burt, A.; Vines, P.; Bennett, A.C.; Pickavance, G.C.; Cooper, D.L.M.; Lewis, S.L.; Phillips, O.L.; Brede, B.; Lau, A.; Herold, M.; McNicol, I.M.; Mitchard, E.T.A.; Coombes, D.; Jackson, T.D.; Makaga, L.; Milamizokou Napo, H.O.; Ngomanda, A.; Ntie, S.; Medjibe, V.; Dimbonda, P.; Soenens, L.; Daelemans, V.; Proux, L.; Nilus, R.; Labrière, N.; Jeffery, K.; Burslem, D.F.R.P.; Clewley, D.; Moffat, D.; Qie, L.; Bartholomeus, H.; Vincent, G.; Barbier, N.; Derroire, G.; Abernethy, K.; Scipal, K.; Disney, M. (2025): ForestScan Project : Terrestrial Laser Scanning (TLS) of FBRMS-03: Kabili-Sepilok, Malaysian Borneo 1ha plot SEP-12, March 2017. NERC EDS Centre for Environmental Data Analysis, 28 March 2025. DOI:10.5285/bb81c82352524df99ddd411f6ca2ec81. https://dx.doi.org/10.5285/bb81c82352524df99ddd411f6ca2ec81
ForestScan Project: Terrestrial Laser Scanning (TLS) of FBRMS-03: Kabili-	TLS	Chavana-Bryant, C.; Wilkes, P.; Yang, W.; Burt, A.; Vines, P.; Bennett, A.C.; Pickavance, G.C.; Cooper,

<p>Sepilok, Malaysian Borneo 1ha plot SEP-30</p> <p>Acquisition date: Mar 2017</p> <p>License type: CC BY 4.0 http://creativecommons.org/licenses/by/4.0/</p>		<p>D.L.M.; Lewis, S.L.; Phillips, O.L.; Brede, B.; Lau, A.; Herold, M.; McNicol, I.M.; Mitchard, E.T.A.; Coombes, D.; Jackson, T.D.; Makaga, L.; Milamizokou Napo, H.O.; Ngomanda, A.; Ntie, S.; Medjibe, V.; Dimbonda, P.; Soenens, L.; Daelemans, V.; Proux, L.; Nilus, R.; Labrière, N.; Jeffery, K.; Burslem, D.F.R.P.; Clewley, D.; Moffat, D.; Qie, L.; Bartholomeus, H.; Vincent, G.; Barbier, N.; Derroire, G.; Abernethy, K.; Scipal, K.; Disney, M. (2025): ForestScan Project : Terrestrial Laser Scanning (TLS) of FBRMS-03: Kabili-Sepilok, Malaysian Borneo 1ha plot SEP-30, March 2017. NERC EDS Centre for Environmental Data Analysis, <i>28 March 2025</i>. DOI:10.5285/ff217c783e3f4c66a4891d2b5807ee6e. https://dx.doi.org/10.5285/ff217c783e3f4c66a4891d2b5807ee6e</p>
<p>Airborne LiDAR and RGB imagery from Sepilok Reserve and Danum Valley in Malaysia</p> <p>Acquisition date: Feb 2020</p> <p>License type: OGL UK 3.0 https://www.nationalarchives.gov.uk/doc/open-government-licence/version/3/</p>	ALS	<p>Coomes, D.A.; Jackson, T.D. (2022): Airborne LiDAR and RGB imagery from Sepilok Reserve and Danum Valley in Malaysia in 2020. NERC EDS Centre for Environmental Data Analysis, <i>03 October 2022</i>. DOI:10.5285/dd4d20c8626f4b9d99bc14358b1b50fe. https://dx.doi.org/10.5285/dd4d20c8626f4b9d99bc14358b1b50fe</p>
<p>ForestScan: Tree census data for FBRMS-03: Kabili-Sepilok, Malaysian Borneo, plots SEP-11, SEP-12 and SEP-30</p> <p>Acquisition date: SEP-11: Jan 2020 SEP-12: Mar 2020 SEP-30: Jun 2021</p> <p>License: CC BY-NC-SA 4.0 http://creativecommons.org/licenses/by-nc-sa/4.0/</p>	Tree census	<p>Chavana-Bryant, C., Wilkes, P., Yang, W., Burt, A., Vines, P., Bennett, A.C., Pickavance, G., Cooper, D.L.M., Lewis, S.L., Phillips, O.L., Brede, B., Lau, A., Herold, M., McNicol, I.M., Mitchard, E.T.A., Barbier, N., Vincent, G., Coomes, D.A., Jackson, T., Makaga, L., Milamizokou Napo, H.O., Ngomanda, A., Ntie, S., Medjibe, V., Dimbonda, P., Soenens, L., Daelemans, V., Bartholomeus, H., Majalap, N., Nilus, R., Labrière, N., Burslem, D.F.R.P., Qie, L., Derroire, G., Proux, L., Abernethy, K., Jeffery, K., Clewley, D., Moffat, D., Scipal, K. and Disney, M. ForestScan: a unique multiscale dataset of tropical forest structure across 3 continents including terrestrial, UAV and airborne LiDAR and in-situ forest census data. ESSD. 2025 DOI: 10.5521/forestplots.net/2025_2 https://doi.org/10.5521/forestplots.net/2025_2</p>

884 **6. Author contributions**

885 All authors provided input towards the writing of this manuscript.
886 C.Ch.-B. wrote the manuscript with significant input from M.D.
887 C.Ch.-B. developed the TLS data processing pipeline.
888 C.Ch.-B. collected, cleaned, processed and curated TLS data.
889 C.Ch.-B. developed the data repositories and ensured data integrity with support from M.D., the CEDA data management team
890 and the ForestPlots and DataVerse database management teams.
891 P.W. developed the TLS data processing pipeline, assisted in the collection of TLS data in FBRMS-02: Lopé, Gabon and its
892 processing.
893 W.Y. developed the TLS data processing pipeline, assisted in the collection of TLS data in FBRMS-01 Paracou, French Guiana
894 and its processing.
895 A.B., and T.J. collected TLS data in FBRMS-03: Kabili-Sepilok, Malaysian Borneo.
896 H.O.M.N. and L.M. provided field logistics and assisted in the collection of TLS data in FBRMS-02: Lopé, Gabon
897 L.S. and V. D. helped collect TLS in FBRMS-02: Lopé, Gabon.
898 K.A., S.N. & A.N. provided logistics and research permit support for FBRMS-02: Lopé, Gabon.
899 P.V. assisted in the processing of TLS data and developing the TLS2trees Processing Scripts.
900 A.C.B. collected census data in FBRMS-01 Paracou, French Guiana and in FBRMS-02: Lopé, Gabon with assistance from
901 D.L.M.C.
902 V.M., P.D, H.O.M.N. and K.J collected the field census data for LPG-01
903 N.L., P.D., H.O.M.N. and K.J. collected the field census data for OKO-01, OKO-02 and OKO-03 in Lopé, Gabon.
904 T.J., D.C. and G.V. planned and funded the ALS data collection in FBRMS-01, Paracou French Guiana.
905 T.J. & D.C. planned and funded the ALS data collection in FBRMS-03, Kabili-Sepilok, Malaysian Borneo.
906 I.M.M. arranged, collected and processed the UAV-LS data collected over FBRMS-02: Lopé, Gabon.
907 B.B., A.L. and H.B. collected, cleaned, processed and curated TLS and UAV-LS data collected at Paracou, French Guiana.
908 N.B., G.V. collected, cleaned, processed and curated TLS and UAV-LS data collected at Paracou, French Guiana.

909 **7. Competing interests**

910 A.B. is an employee and/or shareowner of Sylvera Ltd. All other authors declare that they have no conflict of interest.

911 **8. Acknowledgements**

912 We are indebted to the long-term work of many researchers in funding, establishing and maintaining the field plots that were
913 used in this study. It is not possible to carry out meaningful cal/val measurements of tropical forest biomass for earth

914 observation studies without the logistical support and expertise of the plot PIs and their teams. We thank Dr Noreen Majalap
915 for logistical and research permit support in FBRMS-03, Kabili-Sepilok, Malaysian Borneo. We also thank the Sabah
916 Biodiversity Council for their support with airborne laser scanning data collection in Kabili-Sepilok, access license number:
917 JKM/MBS.1000-2/2 JLD.9 (122). We thank Esther Conway and her team for their outstanding support in developing the
918 ForestScan CEDA dataset collection. We thank Dr Aurora Levesley and Gaëlle Jaouen for their generous support in developing
919 the ForestPlots and DataVerse tree census data packages. Specific data collection activities were funded by the European Space
920 Agency under ESA/ contract No. 4000126857/20/NL/AI. Work in French Guiana benefited from the Investissement d'Avenir
921 grants of the ANR, France (CEBA: ANR-10-LABX-0025). M.D., P.W., C.Ch.-B., W.Y. acknowledge capital funding for TLS
922 equipment from UCL Geography and the NERC National Centre for Earth Observation (NCEO). T.J. and D.C. acknowledge
923 the funding for ALS data collection over FBRMS-01 Paracou, French Guiana in 2019 and FBRMS-03: Kabili-Sepilok,
924 Malaysian Borneo during February 2020 as part of a NERC project grant (NE/S010750/1). I.M.M. was partly funded by a
925 European Research Council Starting Grant (757526) awarded to E.T.A.M. Work in Lopé was supported by core funding from
926 Total Gabon and the EU-ACP ECOFAC VI grant to the Gabon National Parks Agency for logistics, staff and site operations.
927

9. References

929 R package Geomorph: Geometric Morphometric Analyses of 3D Data: <https://rdrr.io/cran/geomorph/man/read.ply.html>, last
 930 access: November 2025.

931 Agence Nationale des Parcs Nationaux (ANPN): Parcs Gabon, Recherche Scientifique:
 932 <https://scienceparcsgabon.weebly.com/>, last access: November 2024.

933 Askne, J. and Santoro, M.: Experiences in boreal forest stem volume estimation from multitemporal C-band InSAR, in: Recent
 934 Interferometry Applications in Topography and Astronomy, 169-194, 2012.

935 Avitabile, V., Herold, M., Henry, M., and Schmullius, C.: Mapping biomass with remote sensing: a comparison of methods
 936 for the case study of Uganda, Carbon balance and management, 6, 1-14, 10.1186/1750-0680-6-7, 2011.

937 Avitabile, V., Herold, M., Heuvelink, G. B., Lewis, S. L., Phillips, O. L., Asner, G. P., Armston, J., Ashton, P. S., Banin, L.,
 938 and Bayol, N.: An integrated pan-tropical biomass map using multiple reference datasets, Global change biology, 22, 1406-
 939 1420, 10.1111/gcb.13139, 2016.

940 Brede, B., Bartholomeus, H. M., Barbier, N., Pimont, F., Vincent, G., and Herold, M.: Peering through the thicket: Effects of
 941 UAV LiDAR scanner settings and flight planning on canopy volume discovery, International Journal of Applied Earth
 942 Observation and Geoinformation, 114, 103056, 10.1016/j.jag.2022.103056, 2022b.

943 Brede, B., Terryn, L., Barbier, N., Bartholomeus, H. M., Bartolo, R., Calders, K., Derroire, G., Moorthy, S. M. K., Lau, A.,
 944 and Levick, S. R.: Non-destructive estimation of individual tree biomass: Allometric models, terrestrial and UAV laser
 945 scanning, Remote Sensing of Environment, 280, 113180, 10.1016/j.rse.2022.113180, 2022a.

946 Burt, A., Disney, M., and Calders, K.: Extracting individual trees from lidar point clouds using treeseg, Methods in Ecology
 947 and Evolution, 10, 438-445, 10.1111/2041-210x.13121, 2019.

948 Burt, A., Calders, K., Cuni-Sanchez, A., Gómez-Dans, J., Lewis, P., Lewis, S. L., Malhi, Y., Phillips, O. L., and Disney, M.:
 949 Assessment of bias in pan-tropical biomass predictions, Frontiers in Forests and Global Change, 3, 12,
 950 10.3389/ffgc.2020.00012, 2020.

951 Calders, K., Verbeeck, H., Burt, A., Origo, N., Nightingale, J., Malhi, Y., Wilkes, P., Raumonen, P., Bunce, R. G., and Disney,
 952 M.: Laser scanning reveals potential underestimation of biomass carbon in temperate forest, Ecological Solutions and
 953 Evidence, 3, e12197, 10.1002/2688-8319.12197, 2022.

954 Chavana-Bryant, C., Wilkes, P., Yang, W., Burt, A., Bennett, A. C., Pickavance, G., Cooper, D., Lewis, S. L., Phillips, O. L.,
 955 Brede, B., Herold, M., McNicol, I. M., Mitchard, E., Barbier, N., Vincent, G., Coomes, D. A., Jackson, T. D., Makaga, L.,
 956 Milamizokou Napo, H. O., Ngomanda, A., Ntie, S., Medjibe, V., Dimbonda, P., Soenens, L., Daelemans, V., Bartholomeus,
 957 H., Majalap, N., Nilus, R., Labriere, N., Burslem, D. F. R. P., Qie, L., Derroire, G., Proux, L., Abernethy, K., Clewley, D.,
 958 Moffat, D., Scipal, K., Vines, P., and Disney, M.: ForestScan: a multiscale dataset of tropical forest structure across 3
 959 continents including terrestrial, UAV and airborne LiDAR and in-situ forest census data [dataset],
 960 10.5285/88a8620229014e0ebacf0606b302112d, 2025.

961 Chave, J., Réjou-Méchain, M., Bürquez, A., Chidumayo, E., Colgan, M. S., Delitti, W. B., Duque, A., Eid, T., Fearnside, P.
 962 M., and Goodman, R. C.: Improved allometric models to estimate the aboveground biomass of tropical trees, Global change
 963 biology, 20, 3177-3190, 10.1111/gcb.12629, 2014.

964 Contributors, P.: PDAL VoxelCenterNearestNeighbor filter, PDAL documentation, available at: [code], 2025.

965 Cuni-Sanchez, A., White, L. J., Calders, K., Jeffery, K. J., Abernethy, K., Burt, A., Disney, M., Gilpin, M., Gomez-Dans, J.
 966 L., and Lewis, S. L.: African savanna-forest boundary dynamics: a 20-year study, PLoS One, 11, e0156934,
 967 10.1371/journal.pone.0156934, 2016.

968 de Lima, R. A., Phillips, O. L., Duque, A., Tello, J. S., Davies, S. J., de Oliveira, A. A., Muller, S., Honorio Coronado, E. N.,
969 Vilanova, E., and Cuni-Sanchez, A.: Making forest data fair and open, *Nature Ecology & Evolution*, 6, 656-658,
970 10.1038/s41559-022-01738-7, 2022.

971 Demol, M., Calders, K., Krishna Moorthy, S. M., Van den Bulcke, J., Verbeeck, H., and Gielen, B.: Consequences of vertical
972 basic wood density variation on the estimation of aboveground biomass with terrestrial laser scanning, *Trees*, 35, 671-684,
973 10.1007/s00468-020-02067-7, 2021.

974 Demol, M., Aguilar-Amuchastegui, N., Bernotaite, G., Disney, M., Duncanson, L., Elmendorp, E., Espejo, A., Furey, A.,
975 Hancock, S., and Hansen, J.: Multi-scale lidar measurements suggest miombo woodlands contain substantially more carbon
976 than thought, *Communications Earth & Environment*, 5, 366, 10.1038/s43247-024-01448-x, 2024.

977 Demol, M., Verbeeck, H., Gielen, B., Armston, J., Burt, A., Disney, M., Duncanson, L., Hackenberg, J., Kukenbrink, D., Lau,
978 A., Ploton, P., Sewdien, A., Stovall, A., Takoudjou, S. M., Volkova, L., Weston, C., Wortel, V., and Calders, K.: Estimating
979 forest above-ground biomass with terrestrial laser scanning: Current status and future directions, *Methods in Ecology and
980 Evolution*, 13, 1628-1639, 10.1111/2041-210x.13906, 2022.

981 Derroire, G., Hérault, B., Rossi, V., Blanc, L., Gourlet- Fleury, S., and Schmitt, L.: Paracou forest permanent plots (V3),
982 CIRAD Dataverse [dataset], 10.18167/DVN1/8G8AHY, 2023.

983 Derroire, G., Hérault, B., Rossi, V., Blanc, L., Gourlet-Fleury, S., and Schmitt, L.: ForestScan (DRAFT VERSION), CIRAD
984 Dataverse [dataset], doi/10.18167/DVN1/94XHID, 2025.

985 Open3D library: https://www.open3d.org/docs/0.9.0/tutorial/Basic/file_io.html#mesh, last access: November 2025.

986 Duncanson, L., Armston, J., Disney, M., Avitabile, V., Barbier, N., Calders, K., Carter, S., Chave, J., Herold, M., and Crowther,
987 T. W.: The importance of consistent global forest aboveground biomass product validation, *Surveys in geophysics*, 40, 979-
988 999, 10.1007/s10712-019-09538-8, 2019.

989 Duncanson, L., Kellner, J. R., Armston, J., Dubayah, R., Minor, D. M., Hancock, S., Healey, S. P., Patterson, P. L., Saarela,
990 S., and Marselis, S.: Aboveground biomass density models for NASA's Global Ecosystem Dynamics Investigation (GEDI)
991 lidar mission, *Remote Sensing of Environment*, 270, 112845, 10.1016/j.rse.2021.112845, 2022.

992 Editorial: We must get a grip on forest science-before it's too late, *Nature*, 608, 449, 10.1038/d41586-022-02182-0, 2022.

993 Fischer, F. J., Jackson, T., Vincent, G., and Jucker, T.: Robust characterisation of forest structure from airborne laser
994 scanning—A systematic assessment and sample workflow for ecologists, *Methods in ecology and evolution*, 15, 1873-1888,
995 10.1111/2041-210x.14416, 2024.

996 ForestPlots.net, Blundo, C., Carilla, J., Grau, R., Malizia, A., Malizia, L., Osinaga-Acosta, O., Bird, M., Bradford, M.,
997 Catchpole, D., and Ford, A.: Taking the pulse of Earth's tropical forests using networks of highly distributed plots, *Biological
998 Conservation*, 260, 108849, 10.1016/j.biocon.2020.108849, 2021.

999 RIEGL Laser Measurement Systems GmbH: <https://www.riegl.co.uk/>, last access: 01/01/2025.

1000 Goodman, R. C., Phillips, O. L., and Baker, T. R.: The importance of crown dimensions to improve tropical tree biomass
1001 estimates, *Ecological Applications*, 24, 680-698, 10.1890/13-0070.1, 2014.

1002 Jackson, T. D., Fischer, F. J., Vincent, G., Gorgens, E. B., Keller, M., Chave, J., Jucker, T., and Coomes, D. A.: Tall Bornean
1003 forests experience higher canopy disturbance rates than those in the eastern Amazon or Guiana shield, *Global Change Biology*,
1004 30, e17493, 10.1111/gcb.17493, 2024.

1005 Jucker, T., Caspersen, J., Chave, J., Antin, C., Barbier, N., Bongers, F., Dalponte, M., van Ewijk, K. Y., Forrester, D. I., and
1006 Haeni, M.: Allometric equations for integrating remote sensing imagery into forest monitoring programmes, *Global change
1007 biology*, 23, 177-190, 10.1111/gcb.13388, 2017.

1008 Kellner, J. R., Armston, J., Birrer, M., Cushman, K., Duncanson, L., Eck, C., Falleger, C., Imbach, B., Král, K., and Krůček,
1009 M.: New opportunities for forest remote sensing through ultra-high-density drone lidar, *Surveys in Geophysics*, 40, 959-977,
1010 10.1007/s10712-019-09529-9, 2019.

1011 Krisanski, S., Taskhiri, M. S., Gonzalez Aracil, S., Herries, D., and Turner, P.: Sensor agnostic semantic segmentation of
1012 structurally diverse and complex forest point clouds using deep learning, *Remote Sensing*, 13, 1413, 10.3390/rs13081413,
1013 2021.

1014 Labrière, N., Davies, S. J., Disney, M. I., Duncanson, L. I., Herold, M., Lewis, S. L., Phillips, O. L., Quegan, S., Saatchi, S.
1015 S., and Schepaschenko, D. G.: Toward a forest biomass reference measurement system for remote sensing applications, *Global
1016 Change Biology*, 29, 827-840, 10.1111/gcb.16497, 2023.

1017 Lopez-Gonzalez, G., Lewis, S. L., Burkitt, M., and Phillips, O. L.: ForestPlots.net: a web application and research tool to
1018 manage and analyse tropical forest plot data, *Journal of Vegetation Science*, 22, 610-613, 10.1111/j.1654-1103.2011.01312.x,
1019 2011.

1020 Malhi, Y., Girardin, C., Metcalfe, D. B., Doughty, C. E., Aragão, L. E., Rifai, S. W., Oliveras, I., Shenkin, A., Aguirre-
1021 Gutiérrez, J., and Dahlsjö, C. A.: The Global Ecosystems Monitoring network: Monitoring ecosystem productivity and carbon
1022 cycling across the tropics, *Biological Conservation*, 253, 108889, 10.1016/j.biocon.2020.108889, 2021.

1023 Martin-Ducup, O., Mofack, G., Wang, D., Raumonen, P., Ploton, P., Sonké, B., Barbier, N., Couteron, P., and Pélissier, R.:
1024 Evaluation of automated pipelines for tree and plot metric estimation from TLS data in tropical forest areas, *Annals of botany*,
1025 128, 753-766, 10.1093/aob/mcab051, 2021.

1026 McNicol, I. M., Mitchard, E. T., Aquino, C., Burt, A., Carstairs, H., Dassi, C., Modinga Dikongo, A., and Disney, M. I.: To
1027 what extent can UAV photogrammetry replicate UAV LiDAR to determine forest structure? A test in two contrasting tropical
1028 forests, *Journal of Geophysical Research: Biogeosciences*, 126, e2021JG006586, 10.1029/2021JG006586, 2021.

1029 Momo, S. T., Ploton, P., Martin-Ducup, O., Lehnebach, R., Fortunel, C., Sagang, L. B. T., Boyemba, F., Couteron, P., Fayolle,
1030 A., and Libalah, M.: Leveraging signatures of plant functional strategies in wood density profiles of African trees to correct
1031 mass estimations from terrestrial laser data, *Scientific Reports*, 10, 2001, 10.1038/s41598-020-58733-w, 2020.

1032 Morhart, C., Schindler, Z., Frey, J., Sheppard, J. P., Calders, K., Disney, M., Morsdorf, F., Raumonen, P., and Seifert, T.:
1033 Limitations of estimating branch volume from terrestrial laser scanning, *European Journal of Forest Research*, 143, 687-702,
1034 10.1007/s10342-023-01651-z, 2024.

1035 Ochiai, O., Poulter, B., Seifert, F. M., Ward, S., Jarvis, I., Whitcraft, A., Sahajpal, R., Gilliams, S., Herold, M., and Carter, S.:
1036 Towards a roadmap for space-based observations of the land sector for the UNFCCC global stocktake, *Iscience*, 26, 106489,
1037 10.1016/j.isci.2023.106489, 2023.

1038 QGIS Geographic Information System: <https://qgis.org>, last access: November 2025.

1039 Quegan, S., Le Toan, T., Chave, J., Dall, J., Exbrayat, J.-F., Minh, D. H. T., Lomas, M., D'alessandro, M. M., Paillou, P., and
1040 Papathanassiou, K.: The European Space Agency BIOMASS mission: Measuring forest above-ground biomass from space,
1041 *Remote Sensing of Environment*, 227, 44-60, 10.1016/j.rse.2019.03.032, 2019.

1042 Ramachandran, N., Saatchi, S., Tebaldini, S., d'Alessandro, M. M., and Dikshit, O.: Mapping tropical forest aboveground
1043 biomass using airborne SAR tomography, *Scientific Reports*, 13, 6233, 10.1038/s41598-023-33311-y, 2023.

1044 Raumonen, P., Kaasalainen, M., Åkerblom, M., Kaasalainen, S., Kaartinen, H., Vastaranta, M., Holopainen, M., Disney, M.,
1045 and Lewis, P.: Fast automatic precision tree models from terrestrial laser scanner data, *Remote Sensing*, 5, 491-520,
1046 10.3390/rs5020491, 2013.

1047 Roussel, J.-R., Auty, D., Coops, N. C., Tompalski, P., Goodbody, T. R. H., Sánchez Meador, A., Bourdon, J.-F., de Boissieu,
1048 F., and Achim, A.: lidR: An R package for analysis of Airborne Laser Scanning (ALS) data, *Remote Sensing of Environment*,
1049 251, 112061, <https://doi.org/10.1016/j.rse.2020.112061>, 2020.

1050 Saatchi, S., Chave, J., Labriere, N., Barbier, N., Réjou-Méchain, M., Ferraz, A., and Tao, S.: AfriSAR: Aboveground Biomass
1051 for Lope, Mabounie, Mondah, and Rabi Sites, Gabon [dataset], 10.3334/ORNLDAA/1681, 2019.

1052 Saatchi, S. S., Harris, N. L., Brown, S., Lefsky, M., Mitchard, E. T., Salas, W., Zutta, B. R., Buermann, W., Lewis, S. L., and
1053 Hagen, S.: Benchmark map of forest carbon stocks in tropical regions across three continents, Proceedings of the national
1054 academy of sciences, 108, 9899-9904, 10.1073/pnas.1019576108, 2011.

1055 Sabah Forestry Department: Official Website: <https://forest.sabah.gov.my/>, last access: 14/01/2025.

1056 Schepaschenko, D., Chave, J., Phillips, O. L., Lewis, S. L., Davies, S. J., Réjou-Méchain, M., Sist, P., Scipal, K., Perger, C., and
1057 Herault, B.: The Forest Observation System, building a global reference dataset for remote sensing of forest biomass,
1058 Scientific data, 6, 198, 10.1038/s41597-019-0196-1, 2019.

1059 CloudCompare (3D point cloud and mesh processing software) version 2.13: <https://www.cloudcompare.org>, last access:
1060 November 2025.

1061 Verhelst, T. E., Calders, K., Burt, A., Demol, M., D'hont, B., Nightingale, J., Terryn, L., and Verbeeck, H.: Implications of
1062 Pulse Frequency in Terrestrial Laser Scanning on Forest Point Cloud Quality and Individual Tree Structural Metrics, Remote
1063 Sensing, 16, 4560, 10.3390/rs16234560, 2024.

1064 Vincent, G., Verley, P., Brede, B., Delaire, G., Maurent, E., Ball, J., Clocher, I., and Barbier, N.: Multi-sensor airborne lidar
1065 requires intercalibration for consistent estimation of light attenuation and plant area density, Remote Sensing of Environment,
1066 286, 113442, 10.1016/j.rse.2022.113442, 2023.

1067 White, L., Rogers, M. E., Tutin, C. E., Williamson, E. A., and Fernandez, M.: Herbaceous vegetation in different forest types
1068 in the Lopé Reserve, Gabon: implications for keystone food availability, African Journal of Ecology, 33, 124-141,
1069 10.1111/j.1365-2028.1995.tb00788.x, 1995.

1070 Wilkes, P. and Yang, W.: rxp-pipeline: Tools to transform RIEGL terrestrial LiDAR, Zenodo [code], 2025a.

1071 Wilkes, P. and Yang, W.: mat2ply: Tools for converting QSM data to 3D PLY models., Zenodo [code], 2025b.

1072 Wilkes, P., Krisanski, S., Clewley, D., Moffat, D., and Yang, W.: TLS2trees (Version 0.1) Zenodo [code], 2025.

1073 Wilkes, P., Lau, A., Disney, M., Calders, K., Burt, A., de Tanago, J. G., Bartholomeus, H., Brede, B., and Herold, M.: Data
1074 acquisition considerations for terrestrial laser scanning of forest plots, Remote Sensing of Environment, 196, 140-153,
1075 10.1016/j.rse.2017.04.030, 2017.

1076 Wilkes, P., Disney, M., Armston, J., Bartholomeus, H., Bentley, L., Brede, B., Burt, A., Calders, K., Chavana-Bryant, C.,
1077 Clewley, D., Duncanson, L., Forbes, B., Krisanski, S., Malhi, Y., Moffat, D., Origo, N., Shenkin, A., and Yang, W. X.:
1078 TLS2trees: A scalable tree segmentation pipeline for TLS data, Methods in Ecology and Evolution, 14, 3083-3099,
1079 10.1111/2041-210x.14233, 2023.

1080 Zanne, A. E., Lopez-Gonzalez, G., Coomes, D. A., Ilic, J., Jansen, S., Lewis, S. L., Miller, R. B., Swenson, N. G., Wiemann,
1081 M. C., and Chave, J.: Global wood density database [dataset], 10.5061/dryad.234, 2009.

1082